

Chapter 2

Spray Formation and Penetration

Abstract The conventional understanding of spray formation when liquid leaves the nozzle is based on the analysis of the following stages: development of a jet, conversion of a jet into liquid sheets and ligaments, disintegration of ligaments into relatively large droplets (primary break-up) and break-up of large droplets into smaller ones (secondary break-up). The following stages of spray formation are considered in this chapter: instability of a jet emerging from the nozzle, break-up of droplets, and spray penetration, taking and not taking into account the effect of turbulence. In the case of gasoline direct injection engines the development of sprays is typically accompanied by the formation of vortex ring-like structures. Some new approaches to modelling these structures are discussed. The predicted velocities of displacement of the regions of maximal vorticity in typical gasoline engines are compared with available experimental data where possible.

2.1 Spray Formation

Liquid spray formation is a complex process, many details of which are still not fully understood. Perhaps the most rigorous overviews of these processes are given in [32, 95]. Despite the rather comprehensive nature of these reviews, they can by no means be considered complete. This chapter covers essentially the same topic as [32, 95], but there will be very little, if any, overlap between it and these papers. The focus will be on the engineering relevance of the models, rather than on their in-depth mathematical analysis.

The jet formation starts inside the nozzle which, in the simplest case, is a cylinder, through which liquid is supplied to a chamber. The pressure drop across this cylinder is typically rather high. For example, in the case of Diesel engines it can reach 1.8×10^8 Pa [41] with nozzle diameters between 0.1 and 0.2 mm [16]. The high velocity of the liquid inside the nozzle leads to a considerable local drop in pressure below the vapour saturation pressure. This leads to a well known cavitation phenomenon. Modelling and experimental studies of this phenomenon, which affects the

discharge coefficient of the nozzle, have been widely discussed in the literature (e.g. [22, 52, 59]). The detailed analysis of these topics is beyond the scope of this book. We just mention that a simplified approach to the analysis of cavitating flows based on their hydrodynamic similarity is described in [97], while the most comprehensive model is described in [41]. The authors of the latter paper claim that ‘cavitation modelling has reached a stage of maturity at which it can consistently identify many of the effects of nozzle design on cavitation, thus making a significant contribution to nozzle performance and optimization’. The phenomenon closely related to cavitation is known as superheated atomization [50].

The conventional understanding of spray formation when liquid leaves the nozzle is based on the separation of the following stages: development of a jet, conversion of a jet into liquid sheets and ligaments, disintegration of ligaments into relatively large droplets (primary break-up) and break-up of large droplets into smaller ones (secondary break-up) [24, 83, 85]. Sometimes liquid emerges from the nozzle in the form of liquid sheets, which disintegrate into ligaments and droplets, following the above scheme [143]. In both cases, this scheme (and its various modifications, e.g. [86, 154]), however, turned out to be too crude to describe the actually observed initial stage of spray formation [16, 32, 95] on the one hand, and too complex to turn it into a quantitative mathematical model on the other hand. Alternative approaches to modelling these processes were considered in a number of papers including [62, 79, 96, 146]. In a number of papers the analysis of these processes was based on the Reynolds-Averaged Navier-Stokes (RANS) equations, using commercial CFD codes such as ANSYS FLUENT [38], Direct Numerical Simulation (DNS) and Large Eddy Simulation (LES) [12, 30, 37, 99], level set and Volume of Fluid (VOF) methods [55, 106], coupled LES/VOF technique [152], specially developed axisymmetric boundary element method (BEM) [49], fractal concept [72], combined level-set Volume-of-Fluid (CLSVOF) method [4], and dynamic mesh refinement and step response theory [167].

All quantitative models of spray formation developed so far are based on the assumption that liquid jets emerging from nozzles disintegrate directly into droplets due to the development of jet instabilities [26]. One of the main problems with the analysis of these instabilities lies in the fact that the disturbances of even two-dimensional flows (axisymmetric or plane) need to be considered as three-dimensional in the general case. In the case of plane jets, this problem can be overcome with the help of the Squire theorem [151]. According to this theorem, for any unstable three-dimensional disturbance, there is a corresponding two-Dimensional disturbance (with zero perturbation in the third dimension) that is more unstable [105]. This allows us to seek the stability of the plane jets with a two dimensional disturbance. Unfortunately the same approach has been widely applied to round jets, when these jets’ stability has been studied under the assumption that disturbances are also axisymmetric (e.g. [119, 120]). This approach is not necessarily wrong, but it cannot guarantee that the instability captured this way is the strongest one. A rigorous analysis of this problem, taking into account the three-dimensionality of the round jet disturbances, has been presented in a number of recent papers, including [63, 84, 90, 130, 164]. For experimental studies of jet disintegration see [75].

2.1.1 Classical WAVE Model

Perhaps one of the most widely currently used models of spray formation, known as WAVE model, is based on the temporal stability analysis of the Kelvin-Helmholtz instability for a round liquid jet (density ρ_l) with an inviscid outer gas phase (density ρ_g) [118]. The liquid velocity is assumed to be constant inside the jet and drops to zero at the interface between the liquid and gas phases. Assuming that the disturbances are small, axisymmetric (along the flow and in the radial directions) and are proportional to

$$\propto \exp(ikz + \omega t), \quad (2.1)$$

this stability analysis leads to the following dispersion Equation [119]:

$$\begin{aligned} \omega^2 + 2\nu_l k^2 \omega & \left(\frac{I_1'(kR_j)}{I_0(kR_j)} - \frac{2k\mathcal{L}}{k^2 + \mathcal{L}^2} \frac{I_1(kR_j)}{I_0(kR_j)} \frac{I_1'(\mathcal{L}R_j)}{I_0(\mathcal{L}R_j)} \right) \\ &= \frac{\sigma_s k}{\rho_l R_j^2} \left(1 - R_j^2 k^2 \right) \left(\frac{\mathcal{L}^2 - k^2}{\mathcal{L}^2 + k^2} \right) \frac{I_1(kR_j)}{I_0(kR_j)} \\ &+ \frac{\rho_g}{\rho_l} \left(U_j - \frac{i\omega}{k} \right) \left(\frac{\mathcal{L}^2 - k^2}{\mathcal{L}^2 + k^2} \right) \frac{I_1(kR_j)}{I_0(kR_j)} \frac{K_0(kR_j)}{K_1(kR_j)}, \end{aligned} \quad (2.2)$$

where U_j and R_j are the unperturbed velocity and radius of the jet, k is the wave number assumed to be real, ω is the complex frequency (positive real part of ω describes instability growth), σ_s is the surface tension, ν_l is the liquid kinematic viscosity, $\mathcal{L}^2 = k^2 + \frac{\omega}{\nu_l}$, primes denote differentiation.

The value of U_j can be estimated as:

$$U_j = C_j \sqrt{\frac{2\Delta p}{\rho_l}},$$

where C_j is the jet discharge coefficient, Δp is discharge pressure.

Generating the curve fits of the numerical solution to Eq.(2.2) the following expressions for the maximum growth rate ($\Omega = \max(\text{Re}(\omega))$) and the corresponding wavelength Λ were obtained [118, 148]:

$$\Omega \left[\frac{\rho_l R_j^3}{\sigma_s} \right]^{0.5} = \frac{0.34 + 0.38 \text{We}_g^{1.5}}{(1 + Z)(1 + 1.4T^{0.6})}, \quad (2.3)$$

$$\frac{\Lambda}{R_j} = 9.02 \frac{(1 + 0.45Z^{0.5})(1 + 0.4T^{0.7})}{\left(1 + 0.87 \text{We}_g^{1.67} \right)^{0.6}}, \quad (2.4)$$

where

$$Z = 2\text{We}_l^{0.5}/\text{Re}_l, \quad T = Z\text{We}_g^{0.5}, \quad \text{We}_{l,g} = \rho_{l,g}U_j^2R_j/\sigma_s, \quad \text{Re}_l = 2U_jR_j/\nu_l.$$

Approximations (2.3)–(2.4) are valid for $Z \leq 1$ and $\rho_g/\rho_l \leq 0.1$ [118], which is expected to be satisfied in most engineering applications. Note that there is a typo in the equation corresponding to (2.3) given in [88].

Z is also known as the Ohnesorge number and denoted as

$$\text{Oh} = \nu_l \sqrt{\frac{\rho_l}{R_j \sigma_s}}. \quad (2.5)$$

It does not depend on velocity and shows the effect of viscosity [32]. Note that sometimes Oh is defined based on droplet/jet diameter, rather than radius in the above expression [60].

In many practical applications it can be assumed that $\text{Re}_l \gg 1$, which implies that $Z \ll 1, T \ll 1$. In this case, making a further assumption that $\text{We}_{l,g} \gg 1$, Eqs. (2.3)–(2.4) can be simplified to

$$\Omega \left[\frac{\rho_l R_j^3}{\sigma_s} \right]^{0.5} = 0.38 \text{We}_g^{1.5}, \quad (2.6)$$

$$\frac{\Lambda}{R_j} = 9.806 \frac{1}{\text{We}_g}, \quad (2.7)$$

In the opposite case of a very slow moving jet when $Z \ll 1, T \ll 1, \text{We}_{l,g} \ll 1$, Eq. (2.4) predicts that $\Lambda = 9.02R_j$. This is a well known Rayleigh result, when the most unstable wavelength of the jet satisfies the criterion $kR_j \approx 0.7$ (see Fig. 1.5 of [26]).

This analysis of jet instabilities is not used directly in modelling of the spray formation processes but some of the above results are incorporated into the WAVE model. The latter is built upon the approximation of a jet by a string of droplets emerging from the nozzle with a certain radii R_d greater or equal to R_j . The number density of the droplets is found from the conservation of the liquid flow rate. The velocities of the emerging droplets have two components: z -component, which is close to U_j , and the radial component, perpendicular to the z -axis. The value of the latter component is expected to be proportional to the wave growth rate Ω . Building a dimensionless parameter, based on U_j and Ω , we can anticipate that the maximal deviation of the emerging droplets from the z -axis, described by the angle Θ , can be estimated from the equation [118]:

$$\tan\left(\frac{\Theta}{2}\right) = A_j \frac{\Lambda \Omega}{U_j}, \quad (2.8)$$

where the value of the fitting constant A_j depends on the nozzle design. For sharp entrance constant diameter nozzles, with length to diameter ratios in the range 4–8,

the recommended value of this constant is 0.188 [118]. The axial angle φ was chosen at random in the range $(0, 2\pi)$.

Angle Θ defined by Eq. (2.8) is identified with the spray cone angle. It is assumed that the angles of emerging droplets are initially uniformly distributed between 0 and $\Theta/2$.

When the wavelength Λ is noticeably greater than R_j then the radii of the emerging droplets can be estimated from the conservation of mass condition:

$$\frac{4}{3}\pi R_d^3 = \min \left(\pi R_j^2 \Lambda, \pi R_j^2 \frac{2\pi U_j}{\Omega} \right). \quad (2.9)$$

The first term on the right hand side of (2.9) describes the volume of a cylinder with the radius R_j and height Λ . The second term in this equation contributes when the jet disintegrates over the distance less than Λ (strongly unstable jet). The condition of validity of Eq. (2.9) is generally presented as [118]:

$$B_0 \Lambda > R_j,$$

where constant B_0 is taken to be 0.61 to give agreement with data on droplet sizes in sprays. Note that in many papers, including [118], $\Omega/(2\pi)$ is identified with the disturbance frequency. This is obviously not correct as this parameter refers to wave growth or damping. Equation (2.9) can be rewritten in a more conventional form as [118]:

$$R_d = \min \left(\left[3R_j^2 \Lambda / 4 \right]^{0.33}, \left[3\pi R_j^2 U_j / (2\Omega) \right]^{0.33} \right). \quad (2.10)$$

If

$$B_0 \Lambda \leq R_j \quad (2.11)$$

then the initial diameters of droplets emerging from the nozzle are assumed to be equal to R_j . In contrast to the case when $B_0 \Lambda > R_j$ these droplets are unstable and continue to break-up until their radius reaches the value

$$R_{eq} = B_0 \Lambda. \quad (2.12)$$

If $R_j = R_{eq}$ then droplets emerging from the nozzle are marginally stable. Remembering Eq. (2.7) Condition (2.12) for $R_j = R_{eq}$ can be presented as:

$$We_g = We_{g(cr)} = 9.806 \times 0.61 = 5.98 \approx 6.$$

This is a well known condition for bag break-up. Droplet breaks up when

$$We_g > We_{g(cr)} \equiv 6. \quad (2.13)$$

Note that Condition (2.13) refers to the case when We_g is defined based on droplet radius. If this number is defined based on droplet diameter, then this condition should be presented as $We_g > 12$ (e.g. [13]). In a number of papers the value of $We_{g(cr)}$ was estimated as 5.5 ± 1 (see [166]).

To take into account the effect of the liquid viscosity, Eq. (2.13) was generalised to [166]:

$$We_{g(cr)} = 6 \left(1 + C_1 Oh^{C_2} \right). \quad (2.14)$$

The empirical coefficients C_1 and C_2 , suggested by various authors, are presented and discussed in [166].

Criterion (2.13) is based on the assumption that the viscosity of the ambient gas is equal to zero. If this assumption is relaxed then a new criterion for droplet break-up can be derived based on the hypothesis that the gas boundary layer transmits shear stresses to the liquid, and these stresses lead to the break-up process. The criterion of this break-up, known as stripping break-up, can be presented as [13, 101] (see also [117]):

$$We_g / \sqrt{Re_g} > 0.5. \quad (2.15)$$

Although Criterion (2.15) does not follow from the classical WAVE model assumptions, the stripping break-up analysis is widely used alongside the bag break-up analysis within the framework of the classical WAVE model [121, 122]. This tradition will be followed in our description of this model.

The WAVE model is not designed to describe the details of the break-up process. The only process which it intends to capture is the decrease with time of the average droplet radius described by the equation:

$$\frac{dR_d}{dt} = - \frac{R_d - R_{d(eq)}}{t_{bu}}, \quad (2.16)$$

where t_{bu} is the characteristic break-up time, $R_{d(eq)}$ is the radius of marginally stable droplets, inferred from Eqs. (2.13) or (2.15) (for bag and stripping break-up respectively).

From the physical background of the problem, one would expect that t_{bu} is proportional to R_d/Λ and inversely proportional to Ω . Following [118], these two requirements can be combined in the following equation:

$$t_{bu} = 3.726 \frac{B_1 R_d}{\Lambda \Omega}, \quad (2.17)$$

where B_1 is the fitting constant. Remembering (2.3)–(2.4), in the limits $We_g \rightarrow 0$ and $We_g \rightarrow \infty$ Eq. (2.17) can be simplified to

$$t_{bu} = 1.72 B_1 \sqrt{\frac{\rho_l R_d^3}{2\sigma_s}}, \quad (2.18)$$

$$t_{bu} = \frac{B_1 R_d}{U_d} \sqrt{\frac{\rho_l}{\rho_g}}, \quad (2.19)$$

respectively.

Equation (2.18) with $B_1 = \pi/1.72$ describes the characteristic bag break-up time, while Eq. (2.19) describes the characteristic stripping break-up time [118]. There is much uncertainty regarding the choice of constant B_1 in Eq. (2.19). Nichols [101] assumed that $B_1 = 8$, Reitz and Diwakar [122] considered $B_1 = 20$, while O'Rourke and Amsden [104] suggested that $B_1 = \sqrt{3}$.

Although the stripping break-up is expected to take place at higher We_g in the general case, since Re_g is expected to be much greater than 1, the condition $We_g \rightarrow 0$ does not strictly speaking refer to bag break-up, which takes place at $We_g > 6$. The difference between the actual values of t_{bu} and the one which follows from the condition $We_g \rightarrow 0$ is accounted for by the fitting constants involved in the analysis.

2.1.2 TAB and Stochastic Models

In this section, the models different from the one described in Sect. 2.1.1 are briefly summarised. These are the Taylor Analogy Break-up (TAB) model and Stochastic model.

2.1.2.1 TAB Model

The Taylor Analogy Break-up (TAB) model describes the process in terms of the critical deformation of an oscillating-distorting droplet [103, 104]. The external force is caused by the relative droplet motion, the restoring force is the surface tension force, and the damping term results from the liquid viscosity. It is assumed that break-up occurs when the droplet deformation exceeds $R_d/2$ (the most recent results of the analysis of droplet deformation at low Weber numbers are presented in [43]). The Sauter Mean Radius (SMR) of the product droplets at the moment of break-up is found from the conservation of droplet energy during the break-up process:

$$SMR = \frac{R_d}{\frac{7}{3} + \frac{\rho_l R_d v_{def}}{4\sigma_s}},$$

where R_d is the parent droplet radius, v_{def} is the velocity of droplet deformation at the moment of break-up.

In contrast to the classical WAVE model, in the TAB model, after break-up, the product droplets' radii $R_{d\text{pr}}$ follow the distribution:

$$f(R_{d\text{pr}}) = \frac{1}{R} \exp\left(-\frac{R_{d\text{pr}}}{R}\right),$$

where $\bar{R} = \text{SMR}/3$ is the number averaged product droplet radius.

The spray penetration predicted by the TAB model agrees with the results of measurements described in [58]. At the same time it over-predicts the rate of droplet break-up, and tends to predict smaller droplets close to the injector (cf. [156]). Despite the above mentioned problems, the TAB model is widely used for spray computations, and it is a default break-up model in KIVA 2 code.

2.1.2.2 Stochastic Model

As follows from the previous analysis, the WAVE model is essentially a deterministic model, in which the radii of product droplets are determined by Eq. (2.16). The TAB model has a stochastic element in choosing the radii of product droplets assuming that the distribution function of these droplets is *a priori* given, but it still focuses on sample droplets rather than on the whole spectrum. The model suggested in [46] is based on a completely different approach to break-up modelling. The approach used in this paper is based on the assumption, originally suggested by Kolmogorov [73], that the break-up of parent particles into secondary particles does not depend on the instantaneous sizes of the parent particles. This assumption is obviously not valid when R_d is close to $R_{d(\text{eq})}$. In high pressure injection sprays, characterised by large Weber numbers, the hydrodynamic mechanism of atomisation due to the mean velocity difference at the liquid-gas surface, can be complicated by the impact of turbulent fluctuations on jet break-up [46]. Under such conditions, when the specific mechanism of atomisation and the scale of the break-up length cannot be clearly defined, stochastic approaches to the modelling of break-up become more appropriate than deterministic ones.

It was shown in [46] that in the limit of large times $t \rightarrow \infty$, the general equation for the evolution of the droplet number distribution function $F(R_d)$ can be presented in the form of the Fokker-Planck type equation:

$$\begin{aligned} \frac{\partial F(R_d)}{\partial t} = & \left[-3\langle \ln \alpha \rangle - \frac{9}{2}\langle \ln^2 \alpha \rangle - \frac{\partial}{\partial R_d} R_d \langle \ln \alpha \rangle \right. \\ & \left. + \frac{1}{2} \frac{\partial}{\partial R_d} R_d \frac{\partial}{\partial R_d} R_d \langle \ln^2 \alpha \rangle \right] \nu F(R_d), \end{aligned} \quad (2.20)$$

where

$$\langle \ln^n \alpha \rangle = \int_0^1 \ln^n \alpha \, q(\alpha) \, d\alpha,$$

$\alpha \in [0, 1]$ is the parameter linking the radii of product (R_d) and parent (R_{d0}) droplets ($\alpha = R_d/R_{d0}$), $q(\alpha)d\alpha$ is the normalised probability that the radius of each product droplet is within the range $[\alpha R_d, (\alpha + d\alpha)R_d]$, $\nu = \nu_0 q_0$, ν_0 is the break-up fre-

quency of an individual droplet, q_0 is the average number of droplets produced after each break-up action.

Equation (2.20) depends on two unknown constants $\langle \ln \alpha \rangle$ and $\langle \ln^2 \alpha \rangle$. To reach an agreement between the predictions of this model and the measurements [58], it was assumed that $\langle \ln \alpha \rangle = -1/2$ and $\langle \ln^2 \alpha \rangle = 1$. The frequency of break-up ν was obtained from the relation:

$$\nu = \frac{1}{B_1} \frac{|U|}{R_{d0}} \sqrt{\frac{\rho_g}{\rho_l}}. \quad (2.21)$$

The value of constant $B_1 = \sqrt{3}$ was chosen in order to match experimental data on the stripping break-up of droplets.

Further developments of this model were discussed in a number of more recent papers including [47, 48, 124, 125, 133]. An alternative approach to taking into account the effects of turbulence on droplet break-up within the spectrum analogy break-up (SAB) model is described by Habchi [51].

2.1.3 Modified WAVE Models

Since the classical WAVE model has been described, a number of its modifications have been suggested (e.g. [89]). Some of these modifications are briefly summarised in this section.

2.1.3.1 Rayleigh-Taylor Break-up Based Model

The original Rayleigh-Taylor instability model ignored the effects of viscosity and surface tension [26]. It predicted the instability for all wave lengths of the initial disturbance; the rate of growth of disturbances grew with decreasing wave lengths. This model was generalised in [6] to take into account the effects of viscosity and surface tension. This generalisation of the model led to the prediction of instability in a limited range of wave lengths. In the case when the surface tension is taken into account but viscosity is ignored, the wave length of the most unstable wave was given by the expression:

$$\Lambda_{RT} = 2\pi \sqrt{\frac{3\sigma_s}{a\rho_l}}, \quad (2.22)$$

where σ_s is the surface tension, ρ_l is the liquid density, a is the acceleration perpendicular to the surface.

The rate of growth of the wave at this wave length was estimated to be:

$$\Omega_{RT} = \frac{2a}{3} \left[\frac{a\rho_l}{3\sigma_s} \right]^{1/4}. \quad (2.23)$$

When deriving Eqs. (2.22) and (2.23) it was assumed that $\rho_g \ll \rho_l$.

Equations (2.22) and (2.23) were used for modelling droplet break-up by a number of authors, including [82, 109, 127]. In this case the contribution of gravity to a was ignored and this parameter was estimated as a ratio of the drag force to the mass of droplets. This leads to the following expression [109]:

$$a = \frac{3}{8} C_D \frac{\rho_g U^2}{\rho_l R_d}, \quad (2.24)$$

where C_D is the drag coefficient.

Since the Rayleigh-Taylor instability model and its generalisation were derived under the assumption that the liquid-gas interface is flat, Patterson and Reitz [109] suggested that droplet break-up due to this instability takes place when:

$$2R_d > \Lambda_{RT}. \quad (2.25)$$

Remembering (2.22) and (2.24), this condition can be rewritten as

$$R_d > a_{RT} \frac{\sigma_s}{\rho_g U^2}, \quad (2.26)$$

where $a_{RT} = 32\pi^2/(3C_D)$.

Since a_{RT} is expected to be well above 6 in most practically important cases, Condition (2.26) is expected to be more stringent than the corresponding condition for bag instability (Condition (2.13)). In the case of the Newton flow regime (see [25]) when $C_D = 0.44$, $a_{RT} = 239$. In a number of papers, including [82] the right hand side of Eq. (2.22) is multiplied by an adjustable constant C_{RT} , the value of which varies from 1 to 9. This makes Condition $a_{RT} \gg 6$ even more reliable. This means that the effect of the Rayleigh-Taylor instability can be effectively ignored if the effects of droplet bag break-up are taken into account.

Alternative approaches to modelling bag break-up and liquid film disintegration at droplet bag break-up mode are discussed in [42, 44]. A simplified analytical model for droplet break-up was suggested in [145].

2.1.3.2 Models Based on the Rigid Core Concept

One of the main weaknesses of the classical WAVE model is that it is based on the assumption that the jet disintegrates immediately at the exit of the nozzle. This is not compatible with a number of experimental observations, including spray penetration, discussed below and in the next section. To overcome this problem, a number of authors suggested modified versions of the WAVE model, based on the assumption that the jet behaves as a solid body at the exit of the nozzle over a certain distance from the nozzle. In what follows two of these models are briefly discussed.

In the model suggested in [140] it was assumed that parcels constituting the liquid core experience no drag from the gas and move as a rigid jet (core) at a velocity equal to the instantaneous injection velocity $U = U_j$. This concept was based on the experimental observation that the momentum of the core of a Diesel spray is conserved [134, 142]. Also, Karimi [71] showed experimentally that at early injection times the injection velocity of the jet, estimated from the mass flow rate, is approximately equal to velocity of the jet tip. This model was incorporated into KIVA II CFD code by using a modified version of the collision algorithm of Nordin [102] for droplets in the liquid core and the conventional algorithm by O'Rourke [104] away from the core. The radius of this liquid core was allowed to decrease due to stripping of droplets from its surface. This process continued until its radius became half the radius of the nozzle. After this, the WAVE model with modified values of parameters was activated. These modifications refer to the case of transient jets dominated by acceleration processes.

The decrease in Ω with increasing injection acceleration was taken into account, while it was assumed that the wave length of critical instability Λ was not affected by the transient nature of the flow. At a qualitative level, the decrease in Ω with increasing injection acceleration was related to the observation that flow acceleration is expected to lead to relaminarisation of the flow and thickening of the boundary layer in the gas phase around the jet for a certain range of Reynolds numbers [100]. The increase in the boundary layer thickness was, in turn, expected to stabilise the gas-liquid interface [91]. This implies suppression of instability by flow acceleration. Since $t_{bu} \sim 1/\Omega$, the effect of flow acceleration was accounted for by modifying the expression for B_1 in Eq. (2.17). The following relationship was suggested:

$$B_1 = B_{1\text{st}} + c_1 (a^+)^{c_2}, \quad (2.27)$$

where

$$a^+ = 2\sqrt{\text{Re}} \frac{R_d}{U_{\text{inj}}^2} \frac{dU_{\text{inj}}}{dt}$$

is the acceleration parameter taking into account the effect of flow acceleration; c_1 and c_2 are adjustable constants. In the steady-state limit a^+ is zero and $B_1 = B_{1\text{st}}$. Following Reitz [118], it was assumed that $B_{1\text{st}} = 10$. The acceleration parameter a^+ was constructed by analogy with the local pressure gradient parameter p^+ suggested by [10], assuming the laminar-type dependence of the local skin friction coefficient on the Reynolds number.

In the model suggested by Turner et al. [159] the length of the rigid core was estimated using the following equation:

$$L_b = \min (L_s, L_{bu}), \quad (2.28)$$

where

$$L_s = \int_0^t U_j(t') dt' \quad (2.29)$$

is the penetration length of the solid jet,

$$L_{bu} = \int_{t-t_{bu}}^t c_g(t') dt', \quad (2.30)$$

where c_g is the group velocity of the fastest growing disturbance and t_{bu} is the break-up time estimated based on Eq. (2.19), is the break-up length.

Assuming that $We_g \gg 1$, c_g/U_j was shown to be a constant in the range 0.91 to 0.99 for ρ_g/ρ_l between 0.1 and 0.01. This assumption is consistent with that regarding the validity of (2.19) and is satisfied in many engineering applications, including those in Diesel engines.

At distances larger than L_b the classical WAVE model was activated. This approach was shown to be as accurate as the one suggested in [140], but in contrast to [140], it does not require the specification of two additional constants c_1 and c_2 . Also, in contrast to [140], it does not rely on the hypothesis that jet acceleration leads to stabilization of the jet. As follows from the analysis of the stability of plane jets, described in [157, 158], the effect of acceleration is not expected to be the dominant in the development of jet break-up.

Also, it was shown in [159] that taking into account the effects of gas viscosity by modifying the velocity profile in the gas phase allows larger droplets to be predicted at jet break-up, and gives droplet sizes which are more consistent with the experimental observations.

Among other models based on the rigid core concept we mention those suggested in [1, 165].

2.1.3.3 A Unified Spray Break-up Model

In the previous sections basic principles of constructing the WAVE model and its modifications were described. These principles can be applied to a wide range of sprays, including those used in internal combustion engines and fire extinguishers [147]. Further refinements of this model are essential when quantitative analysis of specific processes is required. These refinements are focused on the description of the process as a whole rather than its individual elements. Thus the models based on these refinements are generally called ‘unified models’. These unified models tend to lose their universality and are applicable for a specific range of parameters including particular shapes of the nozzles. In what follows we will briefly describe one of these models, suggested in [14], focused on internal combustion engine applications.

The primary break-up model used in [14] was originally developed in [61]. The conceptual picture describing this model is schematically presented in Fig. 2.1. This

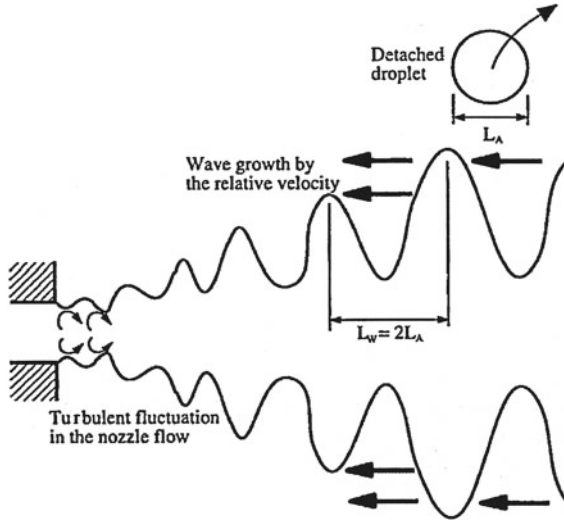


Fig. 2.1 The conceptual picture describing the model of primary break-up, suggested in [61]. Reproduced from Fig. 1 of [61] with permission of Begell House

model considers two main processes: the initial perturbation and wave growth on the jet surface eventually leading to the detachment of droplets.

The model is based on two main assumptions. Firstly, the length scale of atomization (L_A) is proportional to both turbulence length scale (L_t), describing the initial perturbation, and the wavelength (L_w):

$$L_A = C_1 L_t = C_2 L_w. \quad (2.31)$$

Secondly, the time scale of atomization (τ_A) can be expressed as a linear sum of turbulence (τ_t) and wave growth (τ_w) time scales:

$$\tau_A = C_3 \tau_t = C_4 \tau_w. \quad (2.32)$$

Empirical constants C_1 , C_2 , C_3 and C_4 are set to 2.0, 0.5, 1.2 and 0.5 respectively.

Assuming that turbulence can be described by the classical $k - \varepsilon$ model, the initial values of L_t and τ_t are estimated as:

$$L_t = C_\mu \frac{k^{3/2}}{\varepsilon}, \quad (2.33)$$

$$\tau_t = C_\mu \frac{k}{\varepsilon}, \quad (2.34)$$

where $C_\mu = 0.09$, k and ε are the turbulence kinetic energy and dissipation rate [161]. The initial values of k and ε (k_0 and ε_0) are estimated from the balance of forces acting on the flow in the nozzle, taking into account that all forces, except gas inertia and turbulent internal stresses, can be ignored [61]:

$$k_0 = \frac{U^2}{8(L/D)} \left[\frac{1}{C_j} - K_c - (1 - s^2) \right], \quad (2.35)$$

$$\varepsilon_0 = K_\varepsilon \frac{U^3}{2L} \left[\frac{1}{C_j} - K_c - (1 - s^2) \right], \quad (2.36)$$

where L and D are the nozzle length and diameter respectively (typically 3×10^{-4} m and 1.5×10^{-3} m), U is the jet velocity at the nozzle (typically 200 m/s), C_j is the discharge coefficient, introduced in Sect. 2.1.1 (recommended value 0.7), K_ε is the constant taking into account the shape of the nozzle exit (for a sharp entrance corner, typically 0.45), s is the area ratio at the nozzle contraction (recommended value 0.01 [61]).

Assuming that turbulence is homogeneous, the solution to the $k - \varepsilon$ model equations can be presented as [61]:

$$k(t) = \left[\frac{\varepsilon_0}{k_0^{C_\varepsilon}} (C_\varepsilon - 1) t + k_0^{1-C_\varepsilon} \right]^{1/(1-C_\varepsilon)}, \quad (2.37)$$

$$\varepsilon(t) = \varepsilon_0 [k(t)/k_0]^{C_\varepsilon}, \quad (2.38)$$

where $C_\varepsilon = 1.92$ [161].

Having substituted (2.37) and (2.38) into (2.35) and (2.36), the time evolution of L_t and τ_t can be estimated as

$$L_t(t) = L_t^0 \left(1 + \frac{0.0828 t}{\tau_t^0} \right)^{0.457}, \quad (2.39)$$

$$\tau_t(t) = \tau_t^0 + 0.0828 t, \quad (2.40)$$

where t is time since the injection from the nozzle exit, L_t^0 and τ_t^0 are the initial values of L_t and τ_t .

τ_w is estimated as (cf. Eq. (2.19))

$$\tau_w = \frac{L_w}{U} \sqrt{\frac{\rho_l}{\rho_g}}. \quad (2.41)$$

L_w is assumed equal to the wavelength of the fastest growing wave as in the classical WAVE model.

As in the classical WAVE model, the liquid jet is presented in the form of droplet parcels. However, the break-up rate of individual droplets is estimated not based on Eq. (2.16) but based on the following equation:

$$\frac{dR_d}{dt} = -\frac{k_1}{2} \frac{L_A}{\tau_A}, \quad (2.42)$$

where the calibration constant k_1 is chosen to be equal to 0.5 [14].

The drag force, acting on the droplets, emerging from the nozzle, is assumed to be the same as the one acting on the cone shaped liquid core with the drag coefficient equal to 0.3 [14]. The cone half-angle was estimated in [61] as:

$$\tan \frac{\Theta}{2} = \frac{L_A/\tau_A}{U}. \quad (2.43)$$

At the same time, the authors of [14] found that Eq. (2.43) tends to under-estimate the predicted cone angle and suggested that this angle should be doubled, compared with the one predicted by (2.43)

$$\Theta = 4 \tan^{-1} \left(\frac{L_A/\tau_A}{U} \right). \quad (2.44)$$

If the atomiser produces a conical liquid sheet instead of a jet then θ is controlled by the angle of deflection [14]. The liquid sheet instability atomization model, described in [143], was recommended for the analyses of the instability of the liquid sheets [14].

The behaviour of the droplets, formed during the primary break-up, depends mainly on the Weber number We_g , introduced in Eq. (2.3). When $We_g < 6$, the droplets do not break-up directly, but rather deform to form oblate spheroids [14]. At $We_g > 6$ the droplets can undergo secondary break-up. The possibility of the break-up taking place and the type of break-up are controlled both by the values of We_g and the values of the Ohnesorge number, defined by Eq. (2.5). At small Ohnesorge numbers, based on droplet diameters, ($Oh < 0.1$) the transition between break-up regimes depends on We_g only [33]. The following break-up regimes were identified in this range of Oh [14, 18, 33]: bag break-up ($6 < We_g \leq 10$), multimode break-up ($10 < We_g \leq 40$), shear break-up ($40 < We_g \leq 425$) and catastrophic break-up ($We_g > 425$). The threshold values of We_g for these regimes increase as Oh increases, as viscous forces inhibit droplet deformation which is the first step in the break-up process [60], except for catastrophic break-up, when the range does not depend on Oh . In all four break-up regimes the atomization was modelled as a rate process. The detailed analysis of these regimes, incorporation of the relevant models into a numerical code and validation of the results against experimental data for engine application are described and discussed in [14]. Drop properties after secondary break-up at $Oh < 0.039$ were studied experimentally in [60].

Alternative approaches to the multi-scale analysis of liquid atomization processes are described in [23, 27–29, 94]. A review of the most recent primary atomization model, mainly published in issues 11–12 of volume 23 of *Atomization and Sprays*, is presented in [56].

2.2 Spray Penetration

As follows from the analysis presented in the previous subsection, spray formation is a complex process, the details of which are not yet fully understood. This detailed understanding, however, is not always necessary for practical applications of spray models. In many cases, researchers focus just on one aspect of spray behaviour instead of trying to develop a comprehensive universal model. In most cases, this aspect is spray penetration.

The attention to spray penetration has been motivated by three main factors. Firstly, the practical importance of spray penetration (e.g. optimization of spray penetration in internal combustion engines [57]). Secondly, this parameter is easily measurable, so can be used for validation of the models [74]. Thirdly, the correct prediction of the spray penetration can indirectly indicate the correctness of complex models of spray formation.

Models for spray penetration, which have been developed so far, fall into one of two categories. These are the models based on Computational Fluid Dynamics (CFD) codes with sub-models describing jet and droplet break-up processes implemented within them (see Sect. 2.1 and numerous publications including [81]), and simplified models, in which spray penetration has been predicted from first principles. These groups of models are complementary and are sometimes used in parallel. This subsection is focused on the second group of models and they usually allow us to develop better insight into the physical background of the processes. Only axisymmetric jets will be considered. The analysis of the influence of cross winds on the dynamics of sprays was given by Ghosh and Hunt [40].

The problem of spray penetration is closely linked with the problem of induced air velocity within droplet driven sprays. The latter problem was extensively studied by Ghosh and Hunt [39] who considered 3 spray zones: zone 1, where the initial velocities of droplets are much greater than that of the air stream and are not much affected by it; zone 2, where the droplets slow down and their velocities become comparable with the air velocity; zone 3, where the droplets' velocities decrease so much that they become lower than the terminal velocity. These zones, introduced by Ghosh and Hunt [39], have the same physical meanings as mixing, transition and fully developed regions considered by Borman and Ragland [8].

All simplified models suggested so far have been restricted to zones 1 (initial stage) and 3 (fully developed region, which will be referred to as the two-phase flow). The models developed for these zones are considered in the following subsections.

2.2.1 The Initial Stage

The model for the initial stage of spray penetration suggested in [136, 138] is based on the analysis of trajectories of individual droplets formed at the exit of the nozzle. It was assumed that the only force acting on the droplets is the drag force. The

contribution of other forces, including gravity and added mass forces (see [112]) was ignored. This could be justified by the small size of droplets and the fact that droplet density is much greater than ambient air density. The effects of droplet break-up, evaporation and air entrainment were taken into account. As a result, explicit or implicit expressions for spray penetration as functions of time were obtained for the cases of Stokes ($Re_d \leq 2$), Allen ($2 < Re_d \leq 500$) and Newton ($500 < Re_d \leq 10^5$) flows, where Re_d is the droplet Reynolds number based on droplet diameter.

One of the main weaknesses of the model developed in [136, 138] lies in the modelling of air entrainment at the initial stage of spray formation. Following [39], it was assumed that air velocity at this stage is much lower than droplet velocity. This assumption leads to the prediction of strong drag when liquid fuel leaves the nozzle. At the same time, as follows from experimental observations, the mass fraction of air in the vicinity of the nozzle is much lower than the mass fraction of liquid fuel. As a result, air is expected to be almost instantly entrained by liquid fuel in this region. This enables liquid fuel leaving the nozzle to maintain a velocity equal to the injection velocity in the region close to the nozzle. This was taken into account in the models for spray formation described in Sect. 2.1 and allows us to predict the initial spray penetration as

$$s = \int_{t_0}^t v_{inj}(t) dt, \quad (2.45)$$

where $v_{inj}(t)$ is the time dependent injection velocity. Despite its simplicity, Eq. (2.45) is expected to predict the initial spray penetration more accurately than the models described in [136, 138] in most cases.

Roisman et al. [126] drew attention to the fact that jet velocity at the exit from the nozzle can exceed the speed of sound in air c_a . This is expected to lead to the formation of a shock wave in front of the jet. This shock wave was assumed to be one-dimensional and normal to the spray axis, but this is valid only for very short times less than D_0/c_a , where D_0 is the nozzle diameter. It is not clear how the model developed in [126] could be generalised for longer times.

2.2.2 Two-Phase Flow

The analysis of spray penetration is simplified by the fact that zone 3, where droplet velocities are almost equal to ambient air velocities, occupies most of the spray volume. The analysis of droplet and air dynamics in this case can be based on the assumption that droplet and air velocities are equal, thus treating the system droplets-ambient air as a two-phase flow.

Most of the models predicting the penetration of the spray, approximating spray as a two-phase flow, are based on the analysis of the conservation of mass and momentum at various spray cross-sections (e.g. [20, 21, 126, 136]). These models differ by some underlying assumptions, but all of them predict that the dependence

of spray penetration s on time t is close to $s \sim \sqrt{t}$. In what follows, one of the earlier models, suggested in [136], is described. Although this model was developed more than a decade ago, its predictions are still believed to fit experimental data marginally better than the predictions of other similar models (e.g. [162]).

From the equation of conservation of mass of droplets we obtain:

$$\rho_d A_0 v_{in} = \rho_m A_m v_m - (1 - \alpha_d) A_m \rho_g v_m, \quad (2.46)$$

where A_0 is the cross-sectional area of the nozzle, v_{in} is the initial velocity of droplets, ρ_m is the density of a mixture of droplets and gas, A_m is the cross-sectional area of a spray, v_m is the velocity of a mixture.

When deriving Eq. (2.46) and the following equations, the effects of the gradient of droplet number densities and velocities inside the spray in the direction perpendicular to spray axis were ignored. These effects were considered in a number of papers, including [15].

Note that the state of droplets is not important in (2.46) and α_d takes into account the contribution of the gaseous fuel as well. The left hand side of Eq. (2.46) is just the mass flow rate of fuel at the nozzle. The second term in the right hand side of Eq. (2.46) takes into account the contribution of the mass flow rate of entrained air. The first term in the right hand side of this equation gives the mass flow rate of the mixture of fuel and air.

The relation between A_m and A_0 can be presented in the form:

$$A_m = A_0 + \pi D_0 s \tan \theta + \pi s^2 \tan^2 \theta, \quad (2.47)$$

where s is the distance from the nozzle along the axis of the spray, θ is the spray half angle, D_0 is the diameter of the nozzle. When deriving (2.47) it was assumed that $\theta = \text{constant}$. This assumption is similar to the one made by other authors (e.g. [107]). It was relaxed in [135].

From the equation of conservation of momentum:

$$\rho_d A_0 v_{in}^2 = \rho_m A_m v_m^2. \quad (2.48)$$

Equations (2.46)–(2.48) can be combined into the following system of equations:

$$\left. \begin{aligned} \tilde{\rho}_r &= \frac{\tilde{v}}{\tilde{A}} + (1 - \alpha_d) \tilde{\rho}_a \\ \tilde{\rho}_r &= \frac{\tilde{v}^2}{\tilde{A}} \end{aligned} \right\}, \quad (2.49)$$

where the following dimensionless parameters are introduced:

$$\begin{aligned} \tilde{A} &= A_m / A_0 = 1 + \frac{4s \tan \theta}{D_0} + \frac{4s^2 \tan^2 \theta}{D_0^2}; & \tilde{\rho}_r &= \rho_m / \rho_d; \\ \tilde{\rho}_a &= \rho_g / \rho_d; & \tilde{v} &= v_{in} / v_m. \end{aligned}$$

Having eliminated $\tilde{\rho}_r$ from (2.49) the physically meaningful solution is obtained in the form:

$$\tilde{v} = \frac{1}{2} \left(1 + \sqrt{1 + 4(1 - \alpha_d)\tilde{\rho}_a\tilde{A}} \right). \quad (2.50)$$

As follows from (2.50), in the case of no entrained air ($\alpha_d = 1$) we have $\tilde{v} = 1$, which means that $v_m = v_{in}$. This solution, however, does not have a physical meaning since the formation of a spray always includes the entrained air. In a realistic spray environment $\alpha_d \ll 1$.

Remembering the definitions of \tilde{v} and \tilde{A} , the solution (2.50) can be rewritten as:

$$\frac{ds}{dt}|_m = \frac{2v_{in}}{1 + \sqrt{a + bs + cs^2}}, \quad (2.51)$$

where

$$a = 1 + 4(1 - \alpha_d)\tilde{\rho}_a; \quad b = \frac{16(1 - \alpha_d)\tilde{\rho}_a \tan \theta}{D_0}; \quad c = \frac{16(1 - \alpha_d)\tilde{\rho}_a \tan^2 \theta}{D_0^2},$$

subscript m indicates that $\frac{ds}{dt}|_m$ is the velocity of the mixture.

Integration of (2.51) gives:

$$s + \frac{2cs + b}{4c} \sqrt{a + bs + cs^2} - \frac{b\sqrt{a}}{4c} + \frac{4ac - b^2}{8c^{3/2}} \ln \left[\frac{2\sqrt{c(a + bs + cs^2)} + 2cs + b}{2\sqrt{ac} + b} \right] = 2v_{in}t. \quad (2.52)$$

Two limiting cases of Eq. (2.52) were considered, namely: small s ($a \gg bs \gg cs^2$) and large s ($a \ll bs \ll cs^2$). In the case when $a \gg bs \gg cs^2$ (immediate vicinity of the nozzle) Eq. (2.52) is simplified to:

$$s = \frac{2v_{in}t}{1 + \sqrt{a + \frac{b}{8c\sqrt{a}}(a - 1)}} \approx v_{in}t. \quad (2.53)$$

When deriving (2.53) the fact that $\tilde{\rho}_a \ll 1$ and $a - 1 \ll 1$ was taken into account.

Equation (2.53) predicts the expected result that in the immediate vicinity of the nozzle $v_m \approx v_{in}$.

The condition $a \ll bs \ll cs^2$ is satisfied when s is large and/or D_0 is sufficiently small. In these cases Eq. (2.52) is simplified to:

$$s + \frac{s^2\sqrt{c}}{2} \left[1 + \frac{a + 2bs}{2cs^2} \right] - \frac{b\sqrt{a}}{4c} + \frac{4ac - b^2}{8c^{3/2}} \ln \left[\frac{4cs}{2\sqrt{ac} + b} \right] = 2v_{in}t. \quad (2.54)$$

Equation (2.54) can be further simplified if we take into account that:

$$\frac{b}{2\sqrt{ac}} \approx 2\sqrt{\tilde{\rho}_a} \ll 1 \quad (2.55)$$

and reduced to:

$$\frac{s^2\sqrt{c}}{2} + s + \frac{a}{2\sqrt{c}} \left[\frac{1}{2} + \ln \left(\frac{2\sqrt{cs}}{a} \right) \right] = 2v_{\text{in}}t. \quad (2.56)$$

Remembering that $x \gg \ln x$ for large x and keeping the two highest order of magnitude terms in the left hand side of Eq. (2.56) we finally reduce (2.56) to:

$$t \approx \frac{s^2\sqrt{c}}{4v_{\text{in}}} \left(1 + \frac{2}{s\sqrt{c}} \right). \quad (2.57)$$

Equation (2.57) can be rearranged to:

$$s = \frac{\sqrt{v_{\text{in}}D_0t}}{(1 - \alpha_d)^{1/4}\tilde{\rho}_a^{1/4}\sqrt{\tan\theta}} \left(1 - \frac{\sqrt{D_0}}{4\sqrt{v_{\text{in}}}(1 - \alpha_d)^{1/4}\tilde{\rho}_a^{1/4}\sqrt{\tan\theta}\sqrt{t}} \right). \quad (2.58)$$

Equation (2.58) can be further simplified if the second term in the right hand side is ignored thus giving this equation as:

$$s = \frac{\sqrt{v_{\text{in}}D_0t}}{(1 - \alpha_d)^{1/4}\tilde{\rho}_a^{1/4}\sqrt{\tan\theta}}. \quad (2.59)$$

Equation (2.59) for spray penetration is identical to the one suggested by a number of authors (e.g. [19]). From this point of view Eqs. (2.52) and (2.58) can be considered as generalizations of previously discussed formulae. The combination of Eqs. (2.53) and (2.59) gives essentially the same expression for spray penetration as suggested by Lefebvre [83] and Borman and Ragland [8]. For practical applications, however, it seems more appropriate to use the general Eqs. (2.52) and (2.58) rather than their approximate versions (2.53) and (2.59). The main advantage of Eq. (2.52) is that it can accurately predict a smooth transition from the immediate vicinity of the nozzle to the two-phase flow in the region where the spray is fully formed. Separate solutions for the near zone and the far zone discussed in [8, 83] inevitably lead to a physically unrealistic jump in the velocity between these zones (discontinuity of the slope).

The value of v_{in} can be found from the pressure drop at the nozzle (Δp):

$$v_{\text{in}} = C_j\sqrt{2\Delta p/\rho_d}, \quad (2.60)$$

where C_j is the discharge coefficient.

There is some uncertainty regarding the value of C_j . Chehroudi and Bracco [11] recommend $C_j \approx 0.7$, while Lefebvre [83] and Borman and Ragland [8] believe that this value is close to 0.39 (see Eq. (7.7) in [83] and Eq. (9.22a) in [8]; note that there seems to be a printing mistake in Eq. (7.7) in [83]: ρ_A in this equation needs to be replaced by ρ_l , which is the same as ρ_d in our notation).

The spray penetrations predicted by Eqs. (2.52), (2.58) and (2.59) have been compared with the experimental data reported by Allocca et al. [3] (Case 1) and Su et al. [155] (Case 2). The parameter θ (half cone angle) can be estimated based on available theoretical formulae [83], or obtained experimentally from the data in the original papers. The second approach was chosen, as it is more accurate and reliable. This gives the following values: $\theta \approx 13^\circ$ (Case 1) and $\theta \approx 19^\circ$ (Case 2).

As follows from the obtained results (see Fig. 1 of [136]), all three Eqs. (2.52), (2.58) and (2.59) give reasonably accurate predictions of the observed spray penetration. The spray penetration predicted by Eqs. (2.52) and (2.58), however, is noticeably closer to the experimental values than the spray penetration predicted by the simplified Eq. (2.59). Since the results predicted by Eqs. (2.52) and (2.58) are very close, it is recommended that Eq. (2.58) is used for modelling the spray penetration.

Also, the predictions of the above model were shown to be close to the penetration of Diesel spray observed in the rig at Brighton University (UK) and a high-pressure dimethyl ether spray penetration observed at Chungbuk National University (Korea) [139]. This provides additional support to the viability of the model. Also, experimental results reported in [110] show that spray penetration length is approximately proportional to \sqrt{t} . Results of a detailed experimental study of the dependence of liquid phase penetration on the type of fuel used are presented in [108].

Despite encouraging results referring to the comparison between the predictions of the model and experimental data for the cases considered above, this agreement turned out to be far from being universal. For example, Kostas et al. [74] demonstrated that in their experiments $s \sim t^{3/2}$ rather than $s \sim \sqrt{t}$. This and other similar results encouraged us to look for alternative approaches to the modelling of spray penetration. One of such approaches is discussed in the following subsection.

2.2.3 Effects of Turbulence

In the previous subsection, analytical expressions for spray penetration were derived based on equations for conservation of mass and momentum for a two phase flow. A number of simplifying assumptions were made when deriving these equations. Namely, it was assumed that the density of mixture of gas and droplets in the planes perpendicular to spray axis remains constant inside the spray and zero outside it. The shape of the spray boundary was controlled exclusively by the spray cone angle. These assumptions would have been reasonable if the effects of turbulence are ignored. In more realistic cases, when the effects of turbulence are taken into account, their validity becomes questionable. In what follows we describe, following [116], an

approach similar to that discussed in Sect. 2.2.2, but with these two assumptions relaxed.

Instead of assuming that the density of mixture of gas and droplets, spray (ρ_m), is constant in the planes perpendicular to spray axis inside the spray, we assume that it depends on the distance from the spray axis r as:

$$\rho_m = \rho_{m0}(z) \exp \left[-\frac{V_0 r^2}{4D_t z} \right], \quad (2.61)$$

where $\rho_{m0}(z)$ is the mixture density at the axis of the spray, the form of this function does not need to be specified at this stage, D_t is the turbulent diffusion coefficient, V_0 is the initial velocity assumed to be equal to v_{in} (cf. Eq. (2.46)).

Assuming that $\rho_{m0}(z)$ is a weak function of z , Eq. (2.61) predicts that the curves of constant ρ_m correspond to $r \propto \sqrt{z}$. This parabolic form of the spray shape was observed in the experiments [135]. Assuming axial symmetry of the spray and supposing that the velocity of the mixture v_m is constant for given z , we calculate the mass flow rate of the mixture of droplets and gas at the level z as

$$\dot{m} = 2\pi \int_0^\infty v_m \rho_m r \, dr = \frac{4\pi D_t \rho_{m0} v_m z}{V_0} = \rho_{m0} A_m v_m, \quad (2.62)$$

where $A_m = 4\pi D_t z / V_0$ is the effective cross-section of the spray.

Equation (2.62) predicts that the mass flow rate is zero when $z \rightarrow 0$. This means that this equation cannot be applied for small z . At the same time one would be interested in constructing a model which could predict accurate results for large z , but still reasonable ones for $z \rightarrow 0$. This can be achieved by replacing the effective cross-section introduced above with A_m defined as:

$$A_m = A_0 + 4\pi D_t z / V_0, \quad (2.63)$$

where A_0 is the cross-sectional area of the nozzle. In the limit $z \rightarrow \infty$ the contribution of A_0 is expected to be negligibly small, while in the limit $z \rightarrow 0$ Eq. (2.63) reduces to a physically correct statement that $A_m = A_0$.

Ignoring the contribution of air outside of the area A_m and assuming that the relative volume concentration of droplets α_d is small (this assumption is valid everywhere except the immediate vicinity of the nozzle), we can write the equation of conservation of mass in the form almost identical to Eq. (2.46):

$$\rho_d A_0 V_0 = \rho_{m0} A_m v_m - (1 - \alpha_d) A_m \rho_g v_m, \quad (2.64)$$

where A_m is defined by Eq. (2.63), α_d is the volume fraction of droplets, as in Eq. (2.46) (assumed to be small).

In a similar way we can write the equation for conservation of momentum in the form almost identical to Eq. (2.48):

$$\rho_d A_0 V_0^2 = \rho_{m0} A_m v_m^2. \quad (2.65)$$

The combination of Eqs. (2.63), (2.64) and (2.65) gives us the following equation for the velocity of the mixture (cf. Eq. (2.51)):

$$v_m \equiv \frac{dz}{dt}|_m = \frac{2V_0}{1 + \sqrt{a + bz}}, \quad (2.66)$$

where

$$a = 1 + 4(1 - \alpha_d)\tilde{\rho}_a; \quad b = \frac{64(1 - \alpha_d)D_t\tilde{\rho}_a}{V_0 D_0^2}. \quad \tilde{\rho}_a = \rho_g/\rho_d,$$

Integration of Eq. (2.66) gives:

$$3bz + 2(a + bz)^{3/2} = 6V_0bt. \quad (2.67)$$

For sufficiently large z we can assume that $bz \gg a$ and simplify Eq. (2.67) to

$$z = \left(\frac{9V_0^2}{b}\right)^{1/3} t^{2/3} = \frac{V_0}{4} \left(\frac{9D_0^2}{(1 - \alpha_d)\tilde{\rho}_a D_t}\right)^{1/3} t^{2/3}. \quad (2.68)$$

The dependence of z on t can be compared with the one predicted by Eq. (2.59). In the limit $\alpha_d \rightarrow 0$ Eqs. (2.59) and (2.68) predict the same penetration if:

$$D_t = \frac{9}{64} \frac{V_0^{3/2} (\tan \theta)^{3/2} \sqrt{d_0 t}}{\tilde{\rho}_a^{1/4}}. \quad (2.69)$$

Considering the values of parameters for experimental results discussed in [136] (case 1): $V_0 = 318.3$ m/s, $d_0 = 0.2$ mm, $\theta = 13^\circ$, $t = 1$ ms, $\tilde{\rho}_a = 19.7/760 = 0.025$, we obtain $D_t = 0.1$ m²/s. Tentatively, the turbulent diffusivity coefficient can be roughly estimated from the Tchen formula $D_t = \sigma_u^2 T_L^*$ (strictly valid only in homogeneous turbulence for a long time limit). Then the values of $\sigma_u^2 = 2k/3$ and $T_L = \mathcal{O}(k/\varepsilon)$, if experimentally available, can be used for a cross-check of the above number.

There is much uncertainty regarding the experimental observations of spray penetration as discussed in [135]. The general conclusion inferred in [135] is that in the case of low pressure injection sprays the shape of the spray is close to conical and spray penetration is approximately proportional to \sqrt{t} . For the high pressure injection, the shape of the spray is close to parabolic, described by Eq. (2.61). In this case we would expect that spray penetration is fairly well described by Eq. (2.68) and proportional to $t^{2/3}$. We have checked this conclusion using data from a high-speed video recording of a Diesel spray injected at 100 MPa into air with density of 49 kg/m³. The comparison between the results of experimental measurements of

spray penetration and the best fits of experimental data by the curves $\propto t^{1/2}$ and $\propto t^{2/3}$ showed that the $t^{2/3}$ plot provides a noticeably better fit than the $\propto t^{1/2}$ plot. The maximum and mean deviations for the plot $\propto t^{2/3}$ (37.8 and 9.6%) were clearly less than the maximum and mean deviations for the plot $\propto t^{1/2}$ (65.0 and 21.1%) [116]. This supports our approach to linking spray penetration with turbulent dispersion of droplets, although more studies in this direction are needed.

The effects of turbulence on the initial stage of spray penetration were also studied in [116], based on the analysis of turbulent diffusion of the liquid phase (Eulerian approach, see [17]) or turbulent perturbation of individual droplet trajectories (Lagrangian approach, see [114, 115]). In both approaches the analysis was based on the assumption that spray at the initial stage can be approximated as an array of non-interacting droplets. As mentioned in Sect. 2.2.1, this assumption is highly questionable.

Note that spray penetration is closely linked with its momentum flux. Results of detailed numerical and experimental investigation of these fluxes in high pressure Diesel sprays are presented in [113].

Effects of cavitation and nozzle geometry on spray penetration were studied in [149, 150].

The analysis of spray dynamics presented so far has been based mainly on the Eulerian-Lagrangian approach (Eulerian for the carrier phase and Lagrangian for the dispersed phase). An alternative technique for the analysis of this process could make use of vortex-based algorithms (e.g. [80, 160]). In the latter paper such an algorithm was combined with the fully Lagrangian approach to modelling the dispersed phase. This approach is sometimes known as the Osipov method [53]. In the next section the vortex-based approach is used for the analysis of vortex ring-like structures in sprays.

2.3 Vortex Ring-like Structures in Sprays

Our analysis so far has been focused on the basic processes leading to spray formation and penetration, ignoring a number of important details. These details include the oscillations of sprays and the formation/dynamics of vortex ring-like structures near the spray leading edges. The former process was considered in a number of papers, including [123]. The focus of this section will be on the latter phenomenon.

The vortex ring-like structures are not observed for all sprays. For example, they are not observed for sprays in Diesel engine conditions, where liquid fuel is injected into a high pressure gas, except at the very initial stage of the process [16]. At the same time, these structures are typical for gasoline engine sprays, where liquid fuel is injected into gas at pressures close to atmospheric pressure. A typical spray image in gasoline engine-like conditions (direct injection (G-DI) injector [5]) is shown in Fig. 2.2.

As can be seen in Fig. 2.2, the shape of the spray is rather chaotic, but vortex ring-like structures can be clearly recognised. There are some recognisable

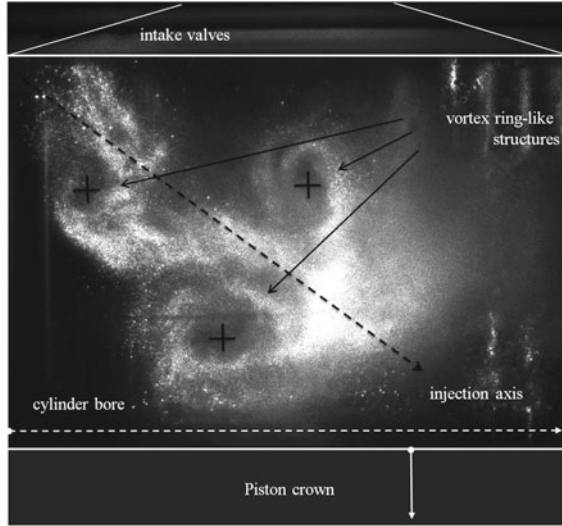


Fig. 2.2 A typical image acquired using a G-DI injector. Positions of the points where radial and axial components of the velocity are equal to zero in the image of the vortex ring are shown as crosses. Reprinted from Ref. [70], Copyright Elsevier (2010)

similarities between these structures and the conventional well organised vortex rings formed, for example, during the injection of water into water with the help of a round piston (e.g. [87, 144]). However, the early attempts to apply the theory of conventional vortex rings to the analysis of the above-mentioned vortex ring-like structures were not successful [137]. In our recent papers [69, 70] the conventional vortex ring theory was generalised to take into account the effect of turbulence. The new model developed in these papers turned out to be successful in predicting some features of the vortex ring-like structures shown in Fig. 2.2, including their translational velocities.

In what follows in this section we will give a brief overview of historic developments of the conventional vortex ring theory. Then recent developments presented in [69, 70] are summarised. Finally, some predictions of the theory developed [69, 70] are compared with experimental data referring to vortex ring-like structures similar to those shown in Fig. 2.2.

2.3.1 Conventional Vortex Rings

A schematic sketch of the vortex ring is presented in Fig. 2.3. R_0 in this figure is the radius of the vortex ring (distance from the vortex ring axis to the area of zero vorticity); ℓ is the characteristic vortex ring thickness. Only the case of a one-phase fluid is considered in this section and the effects of turbulence are ignored. In the

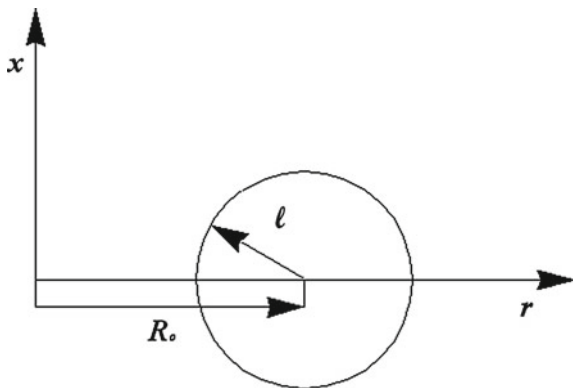


Fig. 2.3 A schematic view of a vortex ring. This figure is reproduced from [141] with permission from JUMV—Society of automotive engineers in Serbia

rest of this section, an overview of historic developments of the conventional vortex ring theory is presented mainly following [70].

Two approaches were used in theoretical studies of vortex ring translational velocities and energies. In the first approach, the relation between velocity and vorticity was used to obtain the formulae for thin cored rings: $\varepsilon = \ell/R_0 \ll 1$ [31, 34]. A more general approach valid for arbitrary ε , developed in [54] (see also [77]), is based on the Helmholtz-Lamb formula for the ring's translational velocity U in the form:

$$U = \frac{\pi}{2M} \int_0^\infty \int_{-\infty}^\infty \left(\Psi - 6x \frac{\partial \Psi}{\partial r} \right) \zeta \, dx \, dr, \quad (2.70)$$

where ζ and Ψ are the vorticity and streamfunction, respectively, and $M = I/\rho$ is the momentum of vorticity per unit density.

Using Eq. (2.70), Saffman [131] (see also [132]) derived an explicit expression for the translational velocity of a thin-cored viscous vortex ring in the form:

$$U_s = \frac{\Gamma_0}{4\pi R_0} \left[\ln \left(\frac{4R_0}{\sqrt{\nu t}} \right) - 0.558 + O \left(\frac{\nu t}{R_0^2} \ln \left(\frac{\nu t}{R_0^2} \right) \right) \right], \quad (2.71)$$

where Γ_0 is the initial circulation of the ring, t is time and ν is the fluid kinematic viscosity. The vorticity distribution inside this ring corresponds to the Lamb-Oseen vortex filament [77]. This asymptotic formula is valid for the description of the initial stage of viscous vortex ring development when $\nu t \ll R_0^2$. The final stage of viscous vortex ring decay ($\nu t \gg R_0^2$) can be described based on the Phillips self-similar solution for the vorticity (ζ_f) and streamfunction (Ψ_f) distributions [111]:

$$\zeta_f = \frac{Mr}{16\pi^{3/2}(\nu t)^{5/2}} \exp\left(-\frac{s_*^2}{2}\right), \quad (2.72)$$

$$\psi_f = \frac{M}{4\pi} \left(\operatorname{erf}\left(\frac{s_*}{\sqrt{2}}\right) - s_* \sqrt{\frac{2}{\pi}} \exp\left(-\frac{s_*^2}{2}\right) \right) \frac{r^2}{(r^2 + x^2)^{3/2}}, \quad (2.73)$$

where

$$s_* = \sqrt{\frac{r^2 + x^2}{2\nu t}},$$

x, r are cylindrical coordinates for the axisymmetric vortex ring. The derivation of the translational velocity in this case is not straightforward. Since Formula (2.70) was derived based on the full Navier-Stokes equation, the substitution of Expressions (2.72) and (2.73) into (2.70) leads to inconsistency.

Attempts to account for the second-order effects of the non-linear convective terms of the vorticity equation were made by Kambe and Oshima [65]. However their results are not uniformly valid. Rott and Cantwell [128, 129] studied this case taking into account the flow dynamics in the potential flow region surrounding the vortical region. They showed that the asymptotic translational velocity of the ring can be predicted by the following formula:

$$U_f = \frac{7M}{15(8\pi\nu t)^{3/2}} = 0.0037038 \frac{I/\rho}{(\nu t)^{3/2}}. \quad (2.74)$$

Another approach to this problem was developed in [7, 64, 67, 68]. These authors obtained a first-order solution to the Navier-Stokes equation with the origin in the centre of the vortex centroid, valid in the limit of small Reynolds numbers Re defined as:

$$\text{Re} = \zeta_0 L^2 / \nu,$$

where $\zeta_0 = At^\lambda$ is the vorticity scale; constant A is to be specified from the conservation of M .

The translational velocity of the viscous vortex ring was derived in the form [67]:

$$U = \frac{M\theta\sqrt{\pi}}{4\pi^2 R_0^3} \left\{ 3 \exp\left(-\frac{\theta^2}{2}\right) I_1\left(\frac{\theta^2}{2}\right) + \frac{\theta^2}{12} {}_2F_2\left(\left\{\frac{3}{2}, \frac{3}{2}\right\}, \left\{\frac{5}{2}, 3\right\}, -\theta^2\right) - \frac{3\theta^2}{5} {}_2F_2\left(\left\{\frac{3}{2}, \frac{5}{2}\right\}, \left\{2, \frac{7}{2}\right\}, -\theta^2\right) \right\}, \quad (2.75)$$

where $\theta = R_0/\ell = \varepsilon^{-1}$, I_1 is the first-order Bessel function and ${}_2F_2$ is the generalised hypergeometric function [98].

Similarly, the kinetic energy and circulation were derived in the form [68]:

$$E = \frac{M^2 \theta \sqrt{\pi}}{2\pi^2 R_0^3} \left\{ \frac{1}{12} {}_2F_2 \left(\left\{ \frac{3}{2}, \frac{3}{2} \right\}, \left\{ \frac{5}{2}, 3 \right\}, -\theta^2 \right) \right\}, \quad (2.76)$$

$$\Gamma = \frac{M}{\pi R_0^2} \left\{ 1 - \exp \left(-\frac{\theta^2}{2} \right) \right\}. \quad (2.77)$$

Note that apart from the definition of Re given above, at least two other definitions of this number, have been used in the literature:

$$\text{Re}_u = U_p D / \nu, \quad (2.78)$$

based on the ejection velocity U_p and orifice diameter D , and

$$\text{Re}_{\Gamma_0} = \Gamma_0 / \nu, \quad (2.79)$$

where Γ_0 is the initial circulation carried by the ring.

The closed-form representations (2.75)–(2.77) enable us to analyse the asymptotic behaviour of these parameters. In the limit of small θ , these equations reduce to:

$$U_f = \frac{M\theta^3}{4\pi^2 R_0^3} \sqrt{\pi} \left(\frac{7}{30} - \frac{11\theta^2}{140} \right) + O(\theta^4), \quad (2.80)$$

$$E_f = \frac{M^2\theta^3}{2\pi^2 R_0^3} \sqrt{\pi} \left(\frac{1}{12} - \frac{\theta^2}{40} \right) + O(\theta^4), \quad (2.81)$$

$$\Gamma_f = \frac{M\theta^2}{2\pi R_0^2}. \quad (2.82)$$

In the limit of large θ , they are reduced to:

$$U_s = \frac{M\sqrt{\pi}}{4\pi^2 R_0^3} \left(\frac{2 \log(\theta) + 3 - \gamma - 2\varphi(3/2)}{2} \right) + O\left(\frac{1}{\theta^4}\right), \quad (2.83)$$

$$E_s = \frac{M^2\sqrt{\pi}}{2\pi^2 R_0^3} (\log(\theta) - \gamma/2 - \varphi(3/2)) + O\left(\frac{1}{\theta^4}\right), \quad (2.84)$$

$$\Gamma_s = \frac{M}{\pi R_0^2}, \quad (2.85)$$

where $\gamma \approx 0.57721566$ is the Euler constant and φ is the di-gamma function defined as

$$\varphi = \frac{d \log \Gamma(x)}{dx},$$

and $\Gamma(x)$ is the Gamma function.

Stanaway et al. [153] performed direct numerical simulation of the Navier-Stokes equation for an axisymmetric vortex ring at small and moderate Reynolds numbers. They showed that Formula (2.75) compares fairly well with their result at a small Reynolds number [35]. The large-Reynolds-number asymptotics was discussed in [36].

An alternative approach to estimate the temporal evolution of the vortex ring translational velocity was suggested by Saffman [131], using simple dimensional analysis. He derived the following equation:

$$U = \frac{M}{k} \left(R_0^2 + k' \nu t \right)^{-3/2}, \quad (2.86)$$

where k and k' are adjustable constants.

To obtain these constants, Weingand and Gharib [163] compared their experimental results for $830 < Re_{\Gamma_0} < 1650$ with those predicted by Eq. (2.86). This comparison led them to the following values: $k = 14.4$ and $k' = 7.8$. Later $k = 10.15$ and $k' = 8.909$ were obtained theoretically by Fukumoto and Kaplanski [35].

2.3.2 Turbulent Vortex Rings

In contrast to the aforementioned laminar vortex ring models, the theory of turbulent vortex rings is far less developed. To the best of the author's knowledge, the first attempt to investigate turbulent vortex ring flow structures was made by Lugovtsov [92, 93] who based his analysis on the introduction of the time-dependent, turbulent (eddy) viscosity (cf. [76, 78]):

$$\nu_* \propto \ell \ell', \quad (2.87)$$

where $\ell' = d\ell/dt$ and $\ell \propto t^{1/4}$. Equation (2.87) follows from a simple dimensional analysis [9], remembering that ℓ has the dimension of length, while ℓ' has the dimension of velocity. Using Eq. (2.87), Lugovtsov [92, 93] developed a turbulent vortex ring model with turbulent viscosity ν_* .

Equations (2.75)–(2.77) were originally derived for $\ell = \sqrt{2\nu t}$ (laminar vortex ring). Later, in [69] it was shown that they remain valid in a more general case when $\ell = at^b$, where a and b are constants ($1/4 \leq b \leq 1/2$). The model based on this presentation of ℓ was called the generalised vortex ring model. This model incorporates both the laminar model for $b = 1/2$ and the fully turbulent model for $b = 1/4$. For $a = \sqrt{2\nu}$, $b = 1/2$ and for large times (small θ), the leading order term of (2.75) is identical with the one predicted by Eq. (2.74). For small times, $\nu t \ll R_0^2$, the vorticity is concentrated on a circle of radius R_0 and tends to a

Gaussian form [67]. The leading term of Expression (2.75) coincides with Saffman's formula (2.71) [35].

For $b = 1/4$ in the generalised vortex ring model, the leading term in (2.80) corresponds to

$$U_f = 0.0105 M t^{-3/4} / a^3. \quad (2.88)$$

The same asymptotic behaviour of the translational velocity for the turbulent vortex ring was found theoretically and tested experimentally in [2, 45]. Some preliminary results of the comparison of the predictions of the above results, referring to the generalised vortex ring model, with the published experimental data were reported in [69].

One of the important limitations of the model described above is that it is based upon the assumption that $R_0 = \text{const}$. Possible alternative approach in which this assumption is relaxed for conventional laminar vortex rings is based on Eq. (2.86). The latter equation was generalised by [69] to take into account the effects of turbulence. These authors started with the dimensionally correct equation:

$$U = \frac{M}{k R^3}, \quad (2.89)$$

where k is a proportionality constant. The decay of circulation can be described by the second dimensionally correct equation:

$$\frac{d(U R)}{dt} = -k' \frac{\nu_* U}{R}, \quad (2.90)$$

where k' is another proportionality constant. The viscosity ν_* is defined by Eq. (2.87). In contrast to the case considered by [131] and [163], ν_* depends on time. Having substituted Eq. (2.89) into Eq. (2.90) and integrating the latter equation from $t = t_0 = 0$ to t , one obtains:

$$R^2 - R_0^2 = \frac{k' a^2}{2} t^{2b}. \quad (2.91)$$

For $b = 1/2$ and $a = \sqrt{2\nu}$, Eq. (2.91) reduces to the one derived by [131] and [163]. Substituting Eq. (2.91) into Eq. (2.89) gives:

$$U = \frac{M}{k (R_0^2 + \frac{k' a^2}{2} t^{2b})^{3/2}}. \quad (2.92)$$

For $b = 1/2$ and $a = \sqrt{2\nu}$, Eq. (2.92) reduces to Eq. (2.86). Hence, Eq. (2.92) can be considered as the generalisation of Eq. (2.86) to the case of arbitrary a and b , including the case of turbulent vortex rings. For further analysis of Eq. (2.92) see the original paper [69].

As follows from the further analysis of the generalised vortex ring model (Eq. (2.75) for $\ell = at^b$ performed in [70], the vorticity distributions, predicted numerically (for realistic $\text{Re} = \zeta_0 L^2/\nu$) and analytically (for $\text{Re} \rightarrow 0$) look rather different. In the numerical results, the contours expand and shift along the axis of symmetry with time, while forms predicted by the analytical solution only expand during the time interval under consideration. Results of calculations of the time evolution of the vortex ring velocities and energies, based on vorticity distributions, predicted by the analytical formulae and numerical solution, however, show that both variables are not sensitive to Re . Hence, analytical formulae are expected to be good approximations for realistic values of vortex ring velocities and energies even for high Reynolds numbers.

The underlying physics behind these effects was clarified by the newly found analytical solution for the normalised vorticity distribution in the limit of long times in the form $\omega_0 + \text{Re}\omega_1$, where ω_0 is the value of vorticity predicted by the classical Phillips solution in the limit $\text{Re} \rightarrow 0$ [111]. Results of further investigations of the effects of Re on vortex rings, leading to the formation of elliptical vortex rings, are described in [66].

As pointed out in [5, 70]. The main advantage of the generalised vortex ring model is that it incorporates an additional parameter b , which can potentially make it applicable to the analysis of not only classical vortex rings, but also complex vortex-ring-like structures similar to those shown in Fig. 2.2. Some results of this comparison for translational velocities of these structures are presented and discussed in the next section.

2.3.3 Translational Velocities of the Vortex Rings-like Structures

The analyses in this section is focused on typical non-evaporating sprays in gasoline engine-like conditions, similar to those shown in Fig. 2.2. The experimental conditions are described in detail in [5]. A summary is presented here, following [70].

Preliminary investigations were performed on two production gasoline injectors; a low pressure port fuel injector (PFI) and a high-pressure, direct injection (G-DI) injector [5]. In both cases, iso-octane was injected into air under atmospheric conditions. High-speed photography was used to observe the formation and translation of vortex ring-like structures. Within both sprays, vortex ring-like structures were observed. However, the most stable and consistent results were obtained in the experiments with the high-pressure injector. In the G-DI spray (see Fig. 2.2), four vortex-ring-like structures could be identified within the experimental data. The two most persistent (and clearly defined) structures were chosen in the comparison with the predictions of the model described in the previous section.

A Dantec Dynamics phase Doppler anemometer (PDA) was used to study the dynamics of fuel droplets in the vortex structures. Measurements of the fuel droplet velocities and diameters were performed in a fine measurement grid that bisected the spray axis and the region of the ring-like structures. The optimisation of the

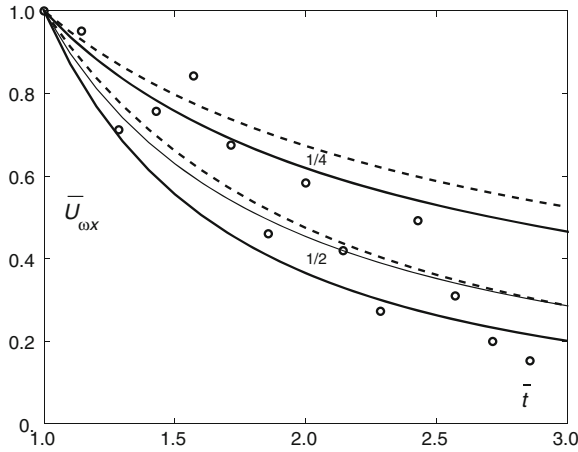


Fig. 2.4 The values of normalised velocities $\tilde{U}_{\omega x}(\tilde{t}) = U_{\omega x}(t)/U_{\omega x}(t_{\text{init}})$ versus normalised time $\tilde{t} = t/t_{\text{init}}$ as obtained from the experimental data (circles), their approximation ($\tilde{U}_{\omega x}(t) = \tilde{t}^{-1.14}$) (thin solid curve) and calculated from Eq.(2.93) for $\tilde{t}_{\text{init}} = t_{\text{init}}/t_0 = 0.5$ (dashed curves) and 5 (thick solid curves), and $b = 1/2$ and $1/4$ (numbers near the curves). Reprinted from Ref. [70], Copyright Elsevier (2010)

PDA operating parameters and the statistical accuracy of the measurements formed an important part of the study. These PDA data were used to study the integral characteristics of the vortex rings including their translational axial velocities.

In Fig. 2.4, the values of the observed axial velocities, normalised by the value of the velocity at the time when the vortex ring was initially observed $\tilde{U}_{\omega x}(\tilde{t}) = U_{\omega x}(t)/U_{\omega x}(t_{\text{init}})$ versus normalised time $\tilde{t} = t/t_{\text{init}}$ are shown by circles. Following [5], the experimental results were approximated by the function $\tilde{U}_{\omega x}(t) = \tilde{t}^{B_n}$, where $B_n = -1.14$ was found using the best fit technique. The plot $\tilde{U}_{\omega x}(t) = \tilde{t}^{-1.14}$ is shown in the same Fig. 2.4.

In [5] these results were compared with the predictions of the generalised vortex ring model in the limit of long times. In what follows, the same comparison is made for arbitrary time, following [70] and using Eq. (2.75). Note that this equation cannot be used directly for comparison with experimental data, as it refers to vortex ring velocity, while the measured variable is the fluid velocity in the region of maximal vorticity $U_{\omega x}(t)$. These two variables are related by the equation [69]:

$$U_{\omega x} \equiv V_{\omega x}/v_n = U_x + 2\pi\theta^2 \int_0^\infty \mu \operatorname{erfc}\left(\frac{\mu}{\sqrt{2}}\right) J_1(\theta\mu) J_0(\sigma_{\text{max}}\mu) d\mu. \quad (2.93)$$

The direct comparison between the experimental results and Eq. (2.93) is still complicated by the fact that the relation of the value of t_{init} and the instant of time the vortex ring is expected to be initiated (t_0) cannot be inferred from experimental data. Following [5], two well separated values of $\tilde{t}_{\text{init}} = t_{\text{init}}/t_0$: $\tilde{t}_{\text{init}} = 0.5$ and $\tilde{t}_{\text{init}} = 5$

were considered, and the corresponding values of $\bar{U}_{\omega x}(\bar{t}) = U_{\omega x}(t)/U_{\omega x}(t_{\text{init}})$ versus \bar{t} for $b = 1/2$ and $b = 1/4$, where $\bar{t} = \tilde{t}/\tilde{t}_{\text{init}} = t/t_{\text{init}}$, were calculated. The plots are shown in the same Fig. 2.4. Note that

$$\bar{t}_{\text{init}} = \frac{t_{\text{init}}}{t_0} = \theta_{\text{init}}^b. \quad (2.94)$$

For $b = 1/2$, the range of \bar{t}_{init} : (0.5, 5) corresponds to the range of θ_{init} : (0.7, 2.2). For $b = 1/4$, the same range of \bar{t}_{init} corresponds to the range of θ_{init} : (0.8, 1, 5).

As follows from Fig. 2.4, most experimental points (8 out of 13) lie between the theoretical curves corresponding to $\bar{t}_{\text{init}} = 5$ and $b = 1/4$ and $1/2$. The points outside this range still look reasonably close to this region remembering the scatter of experimental data. At the same time only 4 out of 13 points lie between the theoretical curves corresponding to $\bar{t}_{\text{init}} = 0.5$ and $b = 1/4$ and $1/2$. Hence, one can conclude that the observed vortex ring-like structures refer to the late stage of vortex ring development with the values of b lying between $b = 1/2$, corresponding to the laminar case, and $b = 1/4$, corresponding to a fully developed turbulent case. The most probable value of $b = 1.14/3 = 0.38$ also lies between $1/4$ and $1/2$.

References

1. Abdelghaffar, W. A., Elwardany, A. E., & Sazhin, S. S. (2010). Modeling of the processes in diesel engine-like conditions: Effects of fuel heating and evaporation. *Atomization Sprays*, 20, 737–737.
2. Afanasyev, Y. D., & Korabel, V. N. (2004). Starting vortex dipoles in a viscous fluid: Asymptotic theory, numerical simulation, and laboratory experiments. *Physics of Fluids*, 16(11), 3850–3858.
3. Allocca, L., Belardini, P., Bertoli, C., Corcione, F. E., & de Angelis, F. (1992). Experimental and numerical analysis of a diesel spray. SAE report 920576.
4. Arienti, M., & Sussman, M. (2014). An embedded level set method for sharp-interface multiphase simulations of diesel injectors. *International Journal of Multiphase Flow*, 59, 1–14.
5. Begg, S., Kaplanski, F., Sazhin, S. S., Hindle, M., & Heikal, M. (2009). Vortex ring structures in gasoline engines under cold-start conditions. *International Journal of Engine Research*, 10, 195–214.
6. Bellman, R., & Pennington, R. H. (1954). Effects of surface tension and viscosity on Taylor instability. *Quarterly of Applied Mathematics*, 12, 151–162.
7. Berezovski, A., & Kaplanski, F. (1995). Vorticity distributions for thick and thin vortex pairs and rings. *Archives of Mechanics*, 47(6), 1015–1026 (in Russian).
8. Borman, G. L., & Ragland, K. W. (1998). *Combustion engineering*. New York: McGraw-Hill.
9. Cantwell, B. (2002). *Introduction to symmetry analysis*. Cambridge: Cambridge University Press.
10. Cebeci, T., & Smith, A. M. O. (1974). *Analysis of turbulent boundary layers. Applied mathematics and mechanics* (Vol. 15). NY: Academic Press.
11. Chehroudi, B., & Bracco, F. V. (1988). Structure of a transient hollow cone spray. SAE report 880522.
12. Chesnel, J., Menard, T., Reveillon, J., & Demoulin, F. -X. (2011). Subgrid analysis of liquid jet atomization. *Atomization Sprays*, 21, 41–67.

13. Chigier, N., & Reitz, R. D. (1998). Regimes of jet breakup and breakup mechanisms (physical aspects). In Kuo, K. K. (Ed.), *Recent advances in spray combustion: Spray atomization and drop burning phenomena* (pp. 109–135). Reston: American Institute of Aeronautics and Astronautics Inc.
14. Chrysosakakis, C., & Assamis, D. N. (2008). A unified fuel spray breakup model for internal combustion engine applications. *Atomization Sprays*, 18, 375–426.
15. Cossali, G. E. (2001). An integral model for gas entrainment into full cone sprays. *Journal of Fluid Mechanics*, 439, 353–366.
16. Crua, C., Shoba, T., Heikal, M., Gold, M., & Higham, C. (2010). High-speed microscopic imaging of the initial stage of Diesel spray formation and primary breakup. SAE Technical Report 2010–01-2247.
17. Csanady, G. T. (1973). *Turbulent diffusion in the environment*. Dordrecht-Holland: D. Reidel Publishing Comp.
18. Dai, Z., & Faith, G. M. (2001). Temporal properties of secondary drop breakup in the multi-mode breakup regime. *International Journal of Multiphase Flow*, 27, 217–236.
19. Dent, J. C. (1971). A basic for the comparison of various experimental methods for studying spray penetration. SAE report 710571.
20. Desantes, J. M., Payri, R., Salvador, F. J., & Gil, A. (2006). Development and validation of a theoretical model for diesel spray penetration. *Fuel*, 85, 910–917.
21. Desantes, J. M., Payri, R., Garcia, J. M., & Salvador, F. J. (2007). A contribution to the understanding of isothermal diesel spray dynamics. *Fuel*, 86, 1093–1101.
22. Desantes, J. M., Payri, R., Salvador, F. J., & de la Morena, J. (2010). Influence of cavitation phenomenon on primary break-up and spray behavior at stationary conditions. *Fuel*, 89, 3033–3041.
23. Devassy, B.M., Habchi, C., & Daniel, E. (2013). A new atomization model for high speed liquid jets using a turbulent, compressible, two-phase flow model and a surface density approach. *Proceedings of ILASS—Europe 2013, 25th European Conference on Liquid Atomization and Spray Systems*, Chania, Greece, 1–4 September 2013, paper 32.
24. Dombrowski, N., & Johns, W. R. (1963). The aerodynamic instability and disintegration of viscous liquid sheets. *Chemical Engineering Science*, 18, 203–214.
25. Douglas, J. F., Gasiorek, J. M., Swaffield, J. A., & Jack, L. B. (2005). *Fluid mechanics* (5th ed.). Singapore: Pearson.
26. Drazin, P. G., & Reid, W. H. (2004). *Hydrodynamic stability* (2nd ed.), Cambridge: Cambridge University Press.
27. Dumouchel, C., & Grout, S. (2009). Application of the scale entropy diffusion to describe a liquid atomization process. *International Journal of Multiphase Flow*, 35, 952–962.
28. Dumouchel, C., & Grout, S. (2011). On the scale diffusivity of a 2-D liquid atomization process analysis. *Physica A*, 390, 1811–1825.
29. Dumouchel, C., & Blaisot, J. -B. (2013) Multi-scale analysis of liquid atomization processes and sprays. *Proceedings of ILASS—Europe 2013, 25th European Conference on Liquid Atomization and Spray Systems*, Chania, Greece, 1–4 September 2013, paper 25.
30. Duret, B., Menard, T., Reveillon, J., & Demoulin, F. X. (2013) Improving primary atomization modelling through DNS of two-phase flows. *Proceedings of ILASS—Europe 2013, 25th European Conference on Liquid Atomization and Spray Systems*, Chania, Greece, 1–4 September 2013, paper 110.
31. Dyson, F. W. (1893). The potential of an anchor ring-part ii. *Philosophical transactions of the Royal Society of London*, A184, 1041–1106.
32. Eggers, J., & Villermaux, E. (2008). Physics of liquid jets. *Reports on Progress in Physics* 616, 79 p.
33. Faeth, G. M., Hsiang, L. -P., & Wu, P. -K. (1995). Structure and breakup properties of sprays. *International Journal of Multiphase Flow*, 21, Suppl., 99–127.
34. Fraenkel, L. E. (1972). Examples of steady vortex rings of small cross-section in an ideal fluid. *Journal of Fluid Mechanics*, 51, 119–135.

35. Fukumoto, Y., & Kaplanski, F. (2008). Global time evolution of an axisymmetric vortex ring at low Reynolds numbers. *Physics of Fluids*, 20, 053103.
36. Fukumoto, Y., & Moffatt, H. K. (2008). Kinematic variational principle for motion of vortex rings. *Physica D*, 237, 2210–2217.
37. Fuster, D., Bagué, A., Boeck, T., Le Moyne, L., Leboissetier, A., Popinet, S., et al. (2009). Simulation of primary atomization with an octree adaptive mesh refinement and VOF method. *International Journal of Multiphase Flow*, 35, 550–565.
38. Ghasemi, A., Barron, R. M., & Balachandar, R. (2014). Spray-induced air motion in single and twin ultra-high injection diesel sprays. *Fuel*, 121, 284–297.
39. Ghosh, S., & Hunt, J. C. R. (1994). Induced air velocity within droplet driven sprays. *Proceedings of the Royal Society of London*, A444, 105–127.
40. Ghosh, S., & Hunt, J. C. R. (1998). Spray jets in a cross-flow. *Journal of Fluid Mechanics*, 365, 109–136.
41. Giannadakis, E., Gavaises, M., & Arcoumanis, C. (2006). Modelling of cavitation in diesel injector nozzles. *Journal of Fluid Mechanics*, 616, 153–193.
42. Girin, A. G. (2012). On the mechanism of inviscid drop breakup at relatively small Weber numbers. *Atomization Sprays*, 22, 921–934.
43. Girin, A. G. (2013). Deformation and acceleration of drop. *Proceedings of ILASS—Europe 2013, 25th European Conference on Liquid Atomization and Spray Systems*, Chania, Greece, 1–4 September 2013, paper 43.
44. Girin, A. G., & Ivanchenko, Y. A. (2012). Model of liquid film disintegration at ‘bag’ mode of drop breakup. *Atomization Sprays*, 22, 935–949.
45. Glezer, A., & Coles, D. (1990). An experimental study of a turbulent vortex ring. *Journal of Fluid Mechanics*, 211, 243–283.
46. Gorokhovski, M. A., & Saveliev, V. L. (2003). Analysis of Kolmogorov’s model of breakup and its application into Lagrangian computation of liquid sprays under air-blast atomisation. *Physics of Fluids*, 15, 184–192.
47. Gorokhovski, M., & Herrmann, M. (2008). Modeling primary atomization. *Annual Review of Fluid Mechanics*, 40(1), 343–366.
48. Gorokhovski, M. A., & Saveliev, V. L. (2008). Statistical universalities in fragmentation under scaling symmetry with a constant frequency of fragmentation. *Journal of Physics D: Applied Physics*, 41, 085405.
49. Grout, S., Dumouchel, C., Cousin, J., & Nuglisch, H. (2007). Fractal analysis of atomizing liquid flows. *International Journal of Multiphase Flow*, 33, 1023–1044.
50. Günther, A., & Wirth, K. -E. (2013). Evaporation phenomena in superheated atomization and its impact on the generated spray. *International Journal of Heat and Mass Transfer*, 64, 952–965.
51. Habchi, C. (2011). The energy spectrum analogy breakup (SAB) model for the numerical simulation of sprays. *Atomization Sprays*, 21, 1033–1057.
52. Habchi, C. (2013). A Gibbs free energy relaxation model for cavitation simulation in Diesel injectors. *Proceedings of ILASS—Europe 2013, 25th European Conference on Liquid Atomization and Spray Systems*, Chania, Greece, 1–4 September 2013, paper 93.
53. Healy, D. P., & Young, J. B. (2005). Full Lagrangian methods for calculating the particle concentration and velocity fields in dilute gas-particle flows. *Proceedings of the Royal Society of London. Series A*, 461, 2197–2225.
54. Helmholtz, H. (1858) On integrals of the hydrodynamical equations which express vortex-motion. P. G. Tait, Trans. with a letter by Lord Kelvin (W. Thompson) in *London Edinburgh and Dublin Philosophy Magazine and Journal of Science*, 33, 485–512 (Fourth series).
55. Herrmann, M. (2011). On simulating primary atomization using the refined level set grid method. *Atomization Sprays*, 21, 283–301.
56. Herrmann, M. (2013). On simulating primary atomization. *Atomization and Sprays*, 23 (11–12), v–ix.
57. Heywood, J. B. (1988). *Internal combustion engines fundamentals*. New York: McGraw-Hill Book Company.

58. Hiroyasu, H. & Kadota, T. (1974). Fuel droplet size distribution in a diesel combustion chamber. SAE Paper 740715.
59. Hong, J. G., Ku, K. W., & Lee, C. -W. (2011). Numerical simulation of the cavitating flow in an elliptical nozzle. *Atomization Sprays*, 21, 237–248.
60. Hsiang, L. -P., & Faeth, G. M. (1993). Drop properties after secondary breakup. *International Journal of Multiphase Flow*, 19, 721–735.
61. Huh, K. Y., Lee, E., & Koo, J. -Y. (1998). Diesel spray atomization model considering nozzle exit turbulence conditions. *Atomization Sprays*, 8, 453–459.
62. Jiang, X., Siamas, G. A., Jagus, K., & Karayiannis, T. G. (2010). Physical modelling and advanced simulations of gas-liquid two-phase jet flows in atomization and sprays. *Progress in Energy Combustion Science*, 36, 131–167.
63. Juniper, M. P. (2008). The effect of confinement on the stability of non-swirling round jet/wake flows. *Journal of Fluid Mechanics*, 605, 227–252.
64. Kaltaev, A. (1982). *Investigation of dynamic characteristics of a vortex ring of viscous fluid. Continuum dynamics* (pp. 63–70). Alma-Ata: Kazah State University (in Russian).
65. Kambe, T., & Oshima, Y. (1975). Generation and decay of viscous vortex rings. *Journal of the Physical Society of Japan*, 38, 271–280.
66. Kaplanski, F., Fukumoto, Y., & Rudi, U. (2012). Reynolds-number effects on vortex ring evolution in a viscous fluid. *Physics Fluids*, 24, 033101.
67. Kaplanski, F., & Rudi, U. (1999). Dynamics of a viscous vortex ring. *International Journal of Fluid Mechanics Research*, 26, 618–630.
68. Kaplanski, F., & Rudi, Y. (2005). A model for the formation of ‘optimal’ vortex rings taking into account viscosity. *Physics of Fluids*, 17, 087101.
69. Kaplanski, F., Sazhin, S. S., Fukumoto, Y., Begg, S., & Heikal, M. (2009). A generalised vortex ring model. *Journal of Fluid Mechanics*, 622, 233–258.
70. Kaplanski, F., Sazhin, S. S., Begg, S., Fukumoto, Y., & Heikal, M. (2010). Dynamics of vortex rings and spray induced vortex ring-like structures. *European Journal of Mechanics - B/Fluids*, 29(3), 208–216.
71. Karimi, K. (2007). Characterisation of multiple-injection diesel sprays at elevated pressures and temperatures. Ph.D. Thesis, University of Brighton, Brighton, United Kingdom.
72. Kolakaluri, R., Li, Y., & Kong, S. -C. (2010). A unified spray model for engine spray simulation using dynamic mesh refinement. *International Journal of Multiphase Flow*, 36, 858–869.
73. Kolmogorov, A. N. (1941). On the log-normal distribution of particle sizes during the breakup process. *Doklady Akademii Nauk SSSR*, 31, 99.
74. Kostas, J., Honnery, D., & Soria, J. (2009). Time resolved measurements of the initial stages of fuel spray penetration. *Fuel*, 88, 2225–2237.
75. Kasyap, T. V., Sivakumar, D., & Raghunandan, B. N. (2009). Flow and breakup characteristics of elliptical liquid jets. *International Journal of Multiphase Flow*, 35, 8–19.
76. Kovaszny, L. S. G., Fujita, H., & Lee, R. L. (1974). Unsteady turbulent puffs. *Advances in Geophysics*, 18B, 253–263.
77. Lamb, H. (1932). *Hydrodynamics*. New York: Dover Publishers.
78. Lavrentiev, M. A., & Shabat, B. V. (1973). *Problems of hydrodynamics and mathematical models*. Moscow: Nauka Publishing House. (in Russian).
79. Lebas, R., Menard, T., Beau, P. A., Berlemont, A., & Demoulin, F. X. (2009). Numerical simulation of primary break-up and atomization: DNS and modelling study. *International Journal of Multiphase Flow*, 35, 247–260.
80. Lebedeva, N. A., Osipov, A. N., & Sazhin, S. S. (2013). A combined fully Lagrangian approach to mesh-free modelling of transient two phase flows. *Atomization Sprays*, 23, 47–69.
81. Lee, C. H., & Reitz, R. D. (2013). CFD simulations of diesel spray tip penetration with multiple injections and with engine compression ratios up to 100:1. *Fuel*, 111, 289–297.
82. Lee, C. S., & Park, S. W. (2002). An experimental and numerical study on fuel atomization characteristics of high-pressure diesel injection sprays. *Fuel*, 81, 2417–2423.
83. Lefebvre, A. H. (1989). *Atomization and sprays*. Bristol, PA: Taylor & Francis.
84. Li, X. (1995). Mechanism of atomisation of a liquid jet. *Atomization Sprays*, 5, 89–105.

85. Li, Y., & Umemura, A. (2014). Two-dimensional numerical investigation on the dynamics of ligament formation by Faraday instability. *International Journal of Multiphase Flow*, 60, 64–75.
86. Lightfoot, M. (2009). Fundamental classification of atomization processes. *Atomization Sprays*, 19, 1065–1104.
87. Lim, T., & Nickels, T. (1995). Vortex rings. In S. I. Green (Ed.), *Fluid vortices* (pp. 95–153). Dordrecht: Kluwer.
88. Lin, S. P., & Rietz, R. D. (1998). Droplet and spray formation from a liquid jet. *Annual Review of Fluid Mechanics*, 30, 85–105.
89. Liu, F.-S., Zhou, L., Sun, B. -G., Li, Z. -J., & Schock, H. J. (2008). Validation and modification of wave spray model for diesel combustion simulation. *Fuel*, 87, 3420–3427.
90. Liu, Z., & Liu, Z. (2006). Linear analysis of three-dimensional instability of non-newtonian liquid jets. *Journal of Fluid Mechanics*, 559, 451–459.
91. Lozano, A., Barreras, F., Hauke, G., & Dopazo, C. (2001). Longitudinal instabilities in an air-blasted liquid sheet. *Journal of Fluid Mechanics*, 437, 143–173.
92. Lugovtsov, B. A. (1970). On the motion of a turbulent vortex ring and its role in the transport of passive contaminant. In *Some problems of mathematics and mechanics* (dedicated to the 70th anniversary of M.A. Lavrentiev) (pp. 182–187), Leningrad: Nauka Publishing House (in Russian).
93. Lugovtsov, B. A. (1976). On the motion of a turbulent vortex ring. *Archives of Mechanics*, 28, 759–766.
94. Malaguti, S., Fontanesi, S., Cantore, G., Montanaro, A., & Allocca, L. (2013). Modelling of primary breakup process of a gasoline direct engine multi-hole spray. *Atomization and Sprays*, 23, 861–888.
95. Marmottant, P., & Villermauz, E. (2004). On spray formation. *Journal of Fluid Mechanics*, 498, 73–111.
96. Martinez, L., Benkenida, A., & Cuenot, B. (2010). A model for the injection boundary conditions in the context of 3D simulation of diesel spray: methodology and validation. *Fuel*, 89, 219–228.
97. Martynov, S. B., Mason, D. J., & Heikal, M. R. (2006). Numerical simulation of cavitation flows based on their hydrodynamic similarity. *International Journal of Engine Research*, 7, 1–14.
98. MATHEMATICA (2007). Book version 6.0.0, Wolfram Research Inc. Available at <http://functions.wolfram.com>. Retrieved July 25, 2008.
99. Ménard, T., Tanguy, S., & Berlemont, A. (2007). Coupling level set/VOF/ghost fluid methods: Validation and application to 3D simulation of the primary break-up of a liquid jet. *International Journal of Multiphase Flow*, 33, 510–524.
100. Narasimha, R., & Sreenivasan, K. R. (1979). Relaminarization of fluid flows. *Advances in Applied Mechanics*, 19, 221–301.
101. Nichols, J. (1972). Stream and droplet breakup by shock waves. In D.T. Harrje & F.H. Reardon (Eds.), *Liquid propellant rocket combustion instability* (pp. 126–128), NASA SP-194, Washington, DC.
102. Nordin, N. (2001). Complex chemistry modeling of Diesel spray combustion, Ph.D. Thesis, Chalmers University of Technology, Gothenburg, Sweden.
103. O'Rourke, P. J. (1981). Collective drop effects on vaporizing liquid sprays. Ph.D. thesis, Princeton University.
104. O'Rourke, P. J., & Amsden, A. A. (1987). The TAB method for numerical calculation of spray droplet breakup. SAE report 872089.
105. Panton, R. L. (1996). *Incompressible flow*. New York, Chichester: John Wiley & Sons Inc.
106. Park, K. S., & Heister, S. D. (2010). Nonlinear modeling of drop size distributions produced by pressure-swirl atomizers. *International Journal of Multiphase Flow*, 36, 1–12.
107. Pastor, J. V., López, J. J., García, J. M., & Pastor, J. M. (2008). A 1D model for the description of mixing-controlled inert diesel sprays. *Fuel*, 87, 2871–2885.

108. Pastor, J. V., Garca-Oliver, J. M., Nerva, J.-G., & Giménez, B. (2011). Fuel effect on the liquid-phase penetration of an evaporating spray under transient diesel-like conditions. *Fuel*, 90, 3369–3381.
109. Patterson, M. A., & Reitz, R. D. (1998). Modelling of the effects of fuel spray characteristics on Diesel engine combustion and emission. SAE report 980131.
110. Payri, R., Salvador, F. J., Gimeno, J., & Zapata, L. D. (2008). Diesel nozzle geometry influence on spray liquid-phase fuel penetration in evaporative conditions. *Fuel*, 87, 1165–1176.
111. Phillips, O. M. (1956). The final period of decay of non-homogeneous turbulence. *Proceedings of the Cambridge Philosophical Society*, 252, 135–151.
112. Poole, D. R., Barengghi, C. F., Sergeev, Y. A., & Vinen, W. F. (2005). The motion of tracer particles in helium II. *Physical Review B*, 71, 064514-1-16.
113. Postrioti, L., Mariani, F., & Battistoni, M. (2012). Experimental and numerical momentum flux evaluation of high pressure diesel spray. *Fuel*, 98, 149–163.
114. Pozorski, J., & Minier, J.-P. (1998). On the Lagrangian turbulent dispersion models based on the Langevin equation. *International Journal of Multiphase Flow*, 24, 913–945.
115. Pozorski, J., & Minier, J.-P. (1999). PDF modeling of dispersed two-phase turbulent flows. *Physical Review E*, 59, 855–863.
116. Pozorski, J., Sazhin, S. S., Waclawczyk, M., Crua, C., Kennaird, D., & Heikal, M. R. (2002). Spray penetration in a turbulent flow. *Flow, Turbulence and Combustion*, 68(2), 153–165.
117. Ranger, A. A., & Nicholls, J. A. (1969). The aerodynamic shattering of liquid drops. *AIAA Journal*, 3, 285–290.
118. Reitz, R. D. (1987). Modelling atomization processes in high-pressure vaporizing sprays. *Atomisation and Spray Technology*, 3, 309–337.
119. Reitz, R. D., & Bracco, F. V. (1982). Mechanism of atomization of a liquid jet. *Physics of Fluids*, 25, 1730–1742.
120. Reitz, R. D., & Bracco, F. V. (2009). Mechanisms of breakup of round jets. In N. Chermisnoff (Ed.), *Encyclopedia of fluid mechanics* (Vol. 3, pp. 012101). Houston: Gulf Publishing (Chapter 10).
121. Reitz, R. D., & Diwakar, R. (1986). Effect of drop breakup on fuel sprays. SAE report 860469.
122. Reitz, R. D., & Diwakar, R. (1987). Structure of high-pressure fuel sprays. SAE report 870598.
123. Rewse-Davis, Z., Nouri, J., Gavaises, M., & Arcoumanis, C. (2013). Near-nozzle instabilities in gasoline direct injection sprays. *Proceedings of ILASS—Europe 2013, 25th European Conference on Liquid Atomization and Spray Systems*, Chania, Greece, 1–4 September 2013, paper 141.
124. Rimbart, N. (2010). Simple model for turbulence intermittencies based on self-avoiding random vortex stretching. *Physical Review E*, 81, 056315.
125. Rimbart, N., Séro-Guillaume, O. (2004). Log-stable laws as asymptotic solutions to a fragmentation equation: Application to the distribution of droplets in a high Weber-number spray. *Physical Review E*, 69, 056316.
126. Roisman, I. V., Araneo, L., & Tropea, C. (2007). Effect of ambient pressure on penetration of a diesel spray. *International Journal of Multiphase Flow*, 33, 904–920.
127. Rotondi, R., Bella, G., Grimaldi, C., & Postrioti, L. (2001). Atomization of high-pressure Diesel spray: experimental validation of a new breakup model. SAE report 2001–01-1070.
128. Rott, N., & Cantwell, B. (1993). Vortex drift. i: Dynamic interpretation. *Physics of Fluids*, A5, 1443–1450.
129. Rott, N., & Cantwell, B. (1993). Vortex drift. ii: The flow potential surrounding a drifting vortical region. *Physics of Fluids*, A5, 1451–1455.
130. Ruo, A. C., Chen, F., & Chang, M. H. (1992). Linear instability of compound jets with nonaxisymmetric disturbances. *Physics of Fluids*, 21, 681–689.
131. Saffman, P. G. (1970). The velocity of viscous vortex rings. *Studies in Applied Mathematics*, 49, 371–380.
132. Saffman, P. G. (1992). *Vortex dynamics*. Cambridge: Cambridge University Press.
133. Sarimeseli, A., & Kelbaliev, G. (2004). Modelling of the break-up of deformable particles in developed turbulent flow. *Chemical Engineering Science*, 59, 1233–1240.

134. Sakaguchi, D., Yamamoto, S., Ueki, H., & Ishdia, M. (2010). Study of heterogeneous structure in diesel fuel spray by using micro-probe L2F. *Journal of Fluid Science and Technology*, 5, 75–85.
135. Savich, S. (2001). Spray dynamics and in-cylinder air motion. Ph.D. Thesis, The University of Brighton.
136. Sazhin, S. S., Feng, G., & Heikal, M. R. (2001). A model for fuel spray penetration. *Fuel*, 80(15), 2171–2180.
137. Sazhin, S. S., Kaplanski, F., Feng, G., Heikal, M. R., & Bowen, P. J. (2001). A fuel spray induced vortex ring. *Fuel*, 80(13), 1871–1883.
138. Sazhin, S. S., Crua, C., Kennaird, D., & Heikal, M. R. (2003). The initial stage of fuel spray penetration. *Fuel*, 82(8), 875–885.
139. Sazhin, S. S., Crua, C., Hwang, J. -S., No, S. -Y., & Heikal, M. (2005). Models of fuel spray penetration. *Proceedings of the Estonian Academy of Sciences: Engineering* 11(2), 154–160.
140. Sazhin, S. S., Martynov, S. B., Kristyadi, T., Crua, C., & Heikal, M. R. (2008). Diesel fuel spray penetration, heating, evaporation and ignition: Modelling versus experimentation. *International Journal of Engineering Systems Modelling and Simulation*, 1, 1–19.
141. Sazhin, S. S., Kaplanski, F., Begg, S., & Heikal, M. (2009). Vortex ring-like structures in gasoline fuel sprays, *Proceedings of the JUMV International Automotive Conference and Exhibition (XXII Science and Motor Vehicles 2009)*, Belgrade 14–16 April 2009, paper 31 (CD). Published by the Society of Automotive Engineers of Serbia.
142. Schugger, C., Meingast, U., & Renz, U. (2000). Time-resolved velocity measurements in the primary breakup zone of a high pressure diesel injection nozzle. *Proceedings of ILASS-Europe*, Darmstadt, Germany (2000).
143. Senecal, P. K., Schmidt, D. P., Nouar, I., Rutland, C. J., Reitz, R. D., & Corradini, M. L. (1999). Modeling high-speed viscous liquid sheet atomization. *International Journal of Multiphase Flow*, 25, 1073–1097.
144. Shariff, K., & Leonard, A. (1992). Vortex rings. *Annual Review of Fluid Mechanics*, 24, 235–279.
145. Sher, I., & Sher, E. (2011). Analytical criterion for droplet breakup. *Atomization and Sprays*, 21, 1059–1063.
146. Shinjo, J., & Umemura, A. (2004). Simulation of liquid jet primary breakup: Dynamics of ligament and droplet formation. *International Journal of Multiphase Flow*, 30, 513–532.
147. Snegirev, A., Talalov, V., Sheinman, I., & Sazhin, S. S. (2011). An enhanced spray model for flame suppression simulations. *Proceedings of the Fifth European Combustion Meeting ECM*, Cardiff, 29th June to 1st July 2011 paper 072–1 (CD).
148. Som, S., & Aggarwal, S. K. (2009). Assessment of atomization models for diesel engine simulations. *Atomization and Sprays*, 19, 885–903.
149. Som, S., & Aggarwal, S. K. (2010). Effects of primary breakup modeling on spray and combustion characteristics of compression ignition engines. *Combustion and Flame*, 157, 1179–1193.
150. Som, S., Ramirez, A. I., Longman, D. E., & Aggarwal, S. K. (2011). Effect of nozzle orifice geometry on spray, combustion, and emission characteristics under diesel engine conditions. *Fuel*, 90, 1267–1276.
151. Squire, H. B. (1933). On the stability for three-dimensional disturbances of viscous fluid flow between parallel walls. *Proceedings of the Royal Society of London*, 142, 621–628.
152. Srinivasan, V., Salazar, A. J., & Saito, K. (2008). Numerical investigation on the disintegration of round turbulent liquid jets using LES/VOF techniques. *Atomization and Sprays*, 18, 571–617.
153. Stanaway, S., Cantwell, B. J., & Spalart, P. R. (1988). A numerical study of viscous vortex rings using a spectral method, NASA Technical Memorandum 101041.
154. Stapper, B. E., Sowa, W. A., & Samuelson, G. S. (1992). An experimental study of the effects of liquid properties on the breakup of a two-dimensional liquid sheet. *ASME Journal of Engineering for Gas Turbines and Power*, 114, 39–45.

155. Su, T. F., Patterson, M. A., Reitz, R. D., & Farrell, P. V. (1996). Experimental and numerical studies of high pressure multiple injection sprays. SAE report 960861.
156. Tanner, F. X. (2004). Development and validation of a cascade atomization and drop breakup model for high-velocity dense sprays. *Atomization and Sprays*, 14, 211–242.
157. Turner, M. R., Healey, J. J., Sazhin, S. S., & Piazzesi, R. (2011). Stability analysis and break-up length calculations for steady planar liquid jets. *Journal of Fluid Mechanics*, 668, 384–411.
158. Turner, M. R., Healey, J. J., Sazhin, S. S., & Piazzesi, R. (2012). Wave packet analysis and break-up length calculations for accelerating planar liquid jets. *Fluid Dynamics Research*, 44(1), article number: 015503, DOI: 10.1088/0169-5983/44/1/015503.
159. Turner, M. R., Sazhin, S. S., Healey, J. J., Crua, C., & Martynov, S. B. (2012). A breakup model for transient diesel fuel sprays. *Fuel*, 97, 288–305.
160. Uchiyama, M. (2009). Numerical simulation of non-evaporating spray jet by the vortex method. *Atomization and Sprays*, 19, 917–928.
161. Versteeg, H. K., & Malalasekera, W. (2007). *An introduction to computational fluid dynamics. The finite volume method* (2nd ed.). Harlow: Pearson Prentice Hall.
162. Vogel, T., Rieß, S., Lutz, M., Wenzing, M., & Leipertz, A. (2011). Comparison of current spray models under high pressure and high temperature engine relevant conditions. *Proceedings of the 24th European Conference on Liquid Atomization and Spray Systems (ILASS)—Europe 2011*, Estoril, Portugal, 5–7 September 2011.
163. Weigand, A., & Gharib, M. (1997). On the evolution of laminar vortex rings. *Experiments in Fluids*, 22, 447–457.
164. Yang, H. Q. (1992). Asymmetric instability of a liquid jet. *Physics of Fluids*, A4, 681–689.
165. Yi, Y., & Reitz, R. D. (2004). Modelling the primary breakup of high-speed jets. *Atomization and Sprays*, 14, 53–80.
166. Zhao, H., Liu, H. -F., Cao, X. -K., Li, W. -F., & Xu, J. -L. (2011). Breakup characteristics of liquid drops in bag regime by a continuous and uniform air jet flow. *International Journal of Multiphase Flow*, 37, 530–534.
167. Zhang, K., Wang, Z., Wang, J., & Wang, Z. (2012). Spray model based on step response theory. *Fuel*, 95, 499–503.

Droplets and Sprays

Sazhin, S.

2014, IX, 345 p. 70 illus. in color. With online
files/update., Hardcover

ISBN: 978-1-4471-6385-5